# HIV-1 genome trafficking initiates APOBEC3G packaging in the cytosol

Jordan T. Becker, Edward L. Evans III, Bayleigh E. Benner, Stephanie L. Fricke, Laura E. Smith, Andra E. Bates, & Nathan M. Sherer*

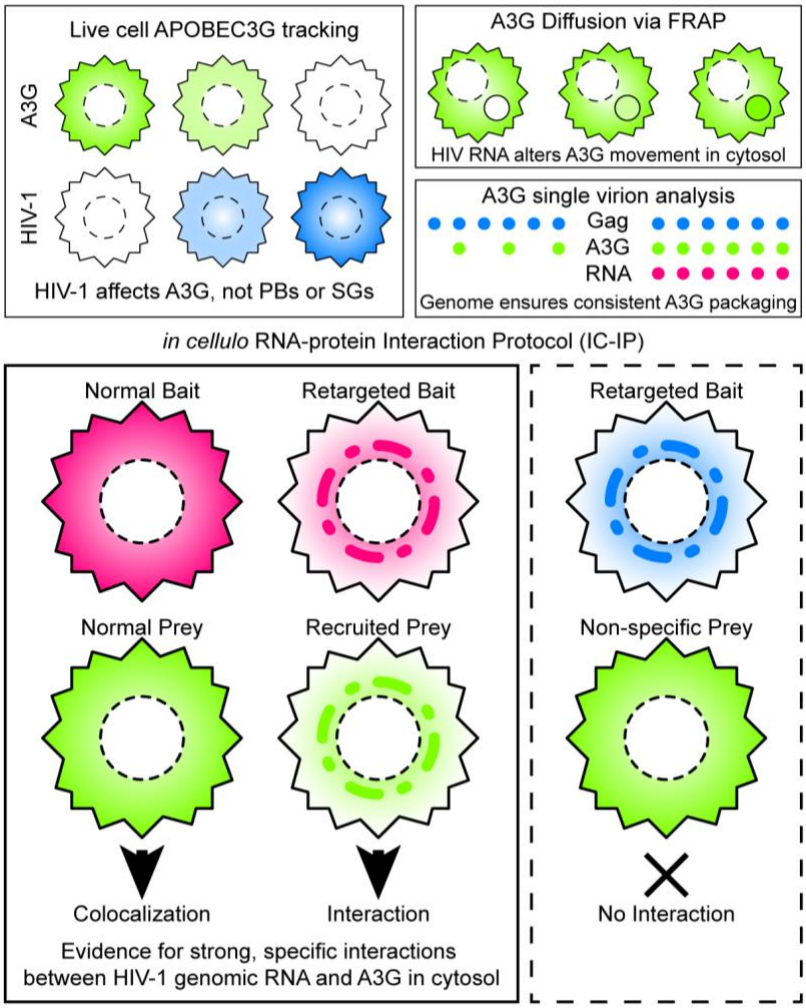


McArdle Laboratory for Cancer Research, Institute for Molecular Virology, and Carbone Cancer Center
University of Wisconsin – Madison
1525 Linden Drive, Madison, WI 53706

Short title: HIV-1 RNA genome regulates A3G trafficking

*To whom correspondence should be addressed: 501 Robert M. Bock Lab, 1525 Linden Drive, Madison, WI 53706. Tel: (608) 890-2551. Email: nsherer@wisc.edu

17 **ABSTRACT**

18 HIV-1 RNA genomes interact with diverse RNA binding proteins in the cytoplasm
19 including antiviral factor APOBEC3G (A3G) that, in the absence of viral Vif proteins, is
20 packaged into virions. When and where genome-A3G interactions are initiated in the host
21 cell is unknown. Here we use quantitative long-term (>24 h) live cell fluorescence video
22 microscopy and a new in-cell RNA-protein interaction assay (the “IC-IP”) to describe
23 subcellular viral and A3G trafficking behaviors over the entire HIV-1 productive phase.
24 Among other findings, we demonstrate that genome-A3G interactions are initiated in the
25 cytosol soon if not immediately after genome nuclear export; that A3G-genome
26 interactions are sufficiently strong so that tethering either factor to membranes inhibits
27 trafficking of the reciprocal binding partner; and that selective recognition of genomes
28 promotes consistent delivery of A3G to sites of virion assembly. Further elucidation of
29 RNA signature(s) detected by A3G may inform development of RNA-targeted antivirals.

30 **INTRODUCTION**

31 The human immunodeficiency virus type 1 (HIV-1) hijacks a diverse set of host
32 cellular RNA binding proteins (RBPs) to carry out viral RNA transcription, nuclear export,
33 translation, and trafficking[1–4]. Select host RBPs are packaged into virions and exhibit
34 antiviral properties, with the best-characterized example being members of the
35 Apolipoprotein B mRNA editing enzyme, catalytic polypeptide-like 3 (APOBEC3) family.
36 A subset of APOBEC3 proteins (A3F, A3G, and A3H) are packaged into virions to abolish
37 infectivity by deaminating cytidines on the nascent minus-sense DNA strand of the viral
38 genome, thereby generating G-to-A mutations in the DNA provirus[5–8]. During productive
39 infection, however, APOBEC3 proteins are counteracted by viral infectivity factor (Vif)
40 proteins that facilitate their proteasome-mediated degradation prior to the onset of virus
41 particle production[9–11].

42 How A3G proteins is delivered to virions in the absence of Vif remains a poorly
43 understood aspect of the cell-intrinsic host defense. HIV-1 virion assembly is driven by
44 viral Gag capsid proteins multimerizing on an RNA scaffold consisting of host-derived
45 RNA molecules and two dimerized viral RNA genomes, with Gag-RNA binding mediated
46 by Gag's C-terminal Nucleocapsid (NC) domain [reviewed in [12]]. In the absence of viral
47 genomes, Gag expression is sufficient to drive formation of non-infectious particles
48 containing cellular RNAs, packaged in proportion to their relative abundance in the
49 cell[13,14]. A3G's incorporation into virions has been shown, for most cell types, to be both
50 RNA- and NC-dependent[15–20]. However, the relative contributions of genomes vs. host
51 RNAs to this process remains controversial. On the one hand, A3G-RNA binding is
52 relatively promiscuous, with A3G incorporated into virus particles even when packageable

53 genomes are not expressed[17,19]. On the other hand, A3G incorporation levels are
54 moderately enhanced when genomes are present[16,21]; and A3G has been shown to
55 exhibit selective RNA-binding characteristics[19,22] including a reported preference for G-
56 rich segments of the HIV-1 genome[20].

57 Where and when A3G interfaces with Gag and/or genomes in the cell has also been
58 under investigation for some time with conflicting results. At steady-state, A3G is
59 distributed throughout the cytosol (the aqueous phase of the cytoplasm) and accumulates
60 to high levels at non-membranous cytoplasmic sites of mRNA decay known as processing
61 bodies (PBs)[23,24]. Cytosolic A3G is also rapidly re-localized to sites of translational
62 repression known as stress granules (SGs) in response to heat shock or oxidative
63 stress[23,24]. Initial studies proposed a functional link between PBs and A3G's antiviral
64 activity[23,25,26]. By contrast, more recent work has shown visible PBs to have little to no
65 discernible relevance to the HIV-1 life cycle[27,28].

66 The dynamic and complex nature of cytoplasmic RNA trafficking during HIV-1 virion
67 genesis may have obscured consistent prior observations made in fixed cells,
68 emphasizing a need for real-time characterization the host RBP response to HIV-1
69 infection at subcellular resolution. Accordingly, herein we set out to comprehensively
70 define the behaviors of HIV-1 RNA genomes, Gag, A3G, and additional PB and SG
71 markers over the entire viral productive phase using long-term (>24h) live cell video
72 microscopy. Our results expose single-cell A3G degradation and trafficking behaviors in
73 the presence or absence of Vif; and show that HIV-1 infection has little to no net effect on
74 cytoplasmic PBs or SG formation. Fluorescence recovery after photobleaching (FRAP)
75 and a new in-cell RNA-protein interaction assay indicate that A3G-genome interactions

76 are strong, specific, Gag-independent, and initiated in a non-localized fashion throughout
77 the cytosol long before the onset of virus particle assembly. Importantly, A3G-genome
78 interactions were sufficiently strong so that artificially tethering A3G to membranes
79 sequestered genomes in the cytoplasm and inhibited HIV-1 virus particle production.
80 Finally, using single virion analysis, we demonstrate that while genomes are not essential
81 for A3G packaging, their presence promotes a more consistent per virion delivery of A3G
82 to sites of virus particle assembly. We discuss the potential implications of A3G's selective
83 recognition of RNA in the host cytosol, and how these principles might be exploited to
84 suppress genome trafficking and virus replication *in vivo*.
85

86 **RESULTS**

87 **Tracking HIV-1 replication using a YFP-A3G biosensor cell line.** To study real-time
88 RBP responses to HIV-1 in single cells over an entire round of viral replication, we
89 generated "biosensor" HeLa cell lines stably expressing fluorescent protein-tagged
90 versions of A3G (YFP-A3G) (Fig 1a) or relevant cytoplasmic RBPs including TIA1-YFP
91 (a marker of SGs) (Fig. 2a) and CFP-DCP1A (a marker of PBs) (Fig. 2e)[24,29]. Cells were
92 infected with either of two versions of an HIV-$1_{NL4-3}$ reporter virus modified to express
93 cyan fluorescent protein (CFP) from the *nef* locus (as a marker of early viral gene
94 expression); either; (1) Vif-competent (Vif+) virus; or (2) a virus rendered Vif-minus (Vifxx)
95 due to insertion of two stop codons in the *vif* reading frame (see cartoon depiction in Fig
96 1b). In the absence of virus, YFP-A3G was localized to the cytoplasm and accumulated
97 in bright foci consistent with PBs, as anticipated (Fig. 1a, left panel). Induction of oxidative
98 stress using 250 μM sodium arsenite (Ars)[30] caused YFP-A3G to accumulate in SGs,
99 confirming an intact stress response (Fig. 1a, right panel). We also confirmed that our
100 YFP-A3G fusion protein was packaged into Vifxx virus particles and retained antiviral
101 activity using single-round assembly and infectivity assays (Fig. 1c).

102 In our first set of live cell imaging experiments, we infected Hela.YFP-A3G cells with
103 Vif+ virus at a MOI of <1 in order to visualize both infected and uninfected cells side-by-
104 side in the same field. Viral gene expression (based on detection of CFP) was initiated
105 12-16 hours post-infection (hpi), followed by a gradual loss of YFP-A3G signal consistent
106 with Vif-dependent YFP-A3G proteasomal degradation (decay rate of 24.5% / h +/-6.0%;
107 n=33; Fig. 1d, Video 1, and quantification in Fig. 1e). We observed YFP-A3G to be
108 depleted from both the diffuse cytosolic and PB pools simultaneously, with levels

109 stabilized at near-background with little to no recovery, even at the latest time points
110 (Fig.1d shows a 48h time point, with Fig.1e showing kinetics over the entire 48h time
111 course). We also observed cell rounding at the latest time points (Fig. 1d and Video 1,
112 see 48 h time point) consistent with real-time visualization of Vif-induced cell cycle
113 arrest[31]. Taken together, these movies validated our use of YFP-A3G as a proxy sensor
114 for detecting HIV-1 infection and tracking multivariate single-cell responses to Vif. Further,
115 they exposed Vif-A3G kinetic details including: (1) that Vif's capacity to degrade A3G is
116 potent in every single infected cell; (2) that Vif operates ubiquitously throughout the
117 cytoplasm; and (3) that Vif's effects are remarkably persistent on a per cell basis, *i.e.*, the
118 YFP-A3G biosensor demonstrated no discernible fluctuations to single-cell Vif activity
119 post-YFP-A3G degradation, even over time frames of greater than 24 h.
120
121 **HIV-1 infection in the absence of Vif re-localizes YFP-A3G to virion assembly sites**
122 **at the plasma membrane.** We next visualized YFP-A3G responses after HeLa.YFP-A3G
123 infection with Vif-deleted (Vifxx) virus. As expected, YFP-A3G expression was maintained
124 in the cytoplasm and at PBs throughout the entire course of infection, and cell cycle arrest
125 was not observed (Fig. 1f and Video 2). Strikingly, however, in infected cells we observed
126 YFP-A3G coalescing in large (up to 4 μm diameter) clusters at 30-48 hpi (Fig. 1f, white
127 arrows highlight growing clusters). These clusters were unlikely to be PBs or SGs based
128 on their proximity to the cell surface and real-time observations of cluster release and
129 transfer to neighboring cells (Fig. 1f, 32h time point, and tracked in Video 2). Instead, we
130 hypothesized that clusters represented recruitment of YFP-A3G from the cytoplasm to
131 sites of virus particle assembly at the plasma membrane. Consistent with this hypothesis,

132 YFP-A3G clusters stained positive for both HIV-1 Gag/Gag-Pol and viral genome but not
133 *YFP-A3G* mRNA (as a negative control) detected using a 4-color combined anti-p24$_{Gag}$
134 immunofluorescence (IF) and RNA fluorescence in situ hybridization (FISH) protocol (Fig.
135 1g). Thin section electron microscopy also confirmed clustering of virus particles at the
136 surface of HeLa.YFP-A3G cells at 48 hpi for both the Vif+ and Vifxx conditions (Fig. 1h).
137 Based on these results, we concluded that even in the absence of Vif, YFP-A3G serves
138 as a useful proxy biosensor for detecting HIV-1 virus particle assembly through monitoring
139 YFP-A3G's virus-driven translocation from the cytoplasm to the plasma membrane.
140
141 **HIV-1 replication has little to no effect on PB integrity or SG formation.** Because
142 HIV-1 drastically alters YFP-A3G subcellular trafficking behaviors in both the presence
143 and absence of Vif expression, we thought it important to ascertain if HIV-1 impacted the
144 net integrity of A3G's major cytoplasmic sites of accumulation, *i.e.*, SGs and PBs. To
145 address this question, we monitored Vif+ and Vifxx HIV-1 infection of two biosensor cell
146 lines engineered to stably express either YFP-TIA1 (Fig. 2a-2c) or CFP-DCP1a (Fig. 2e);
147 validated markers of PBs and SGs, respectively [reviewed in [29]]. We first confirmed that
148 our YFP-TIA1 "stress" biosensor responded to stress similar to YFP-A3G (see Fig. 1a) by
149 treating cells with 250 μM Ars [30] (Fig. 2a, right panel) or infecting cells with rhinovirus A16
150 (RVA16), a positive-strand RNA virus we had studied previously[32] and discovered to
151 cause rampant SG formation as early as 4h post-infection (Fig. 2b and Video 3).
152 Unlike RVA16, neither Vif+ nor Vifxx HIV-1 triggered SG formation in either YFP-
153 TIA1 or YFP-A3G cells over 48h of continuous imaging, a time window sufficient to
154 encompass an entire round of viral replication (Fig. 2c with quantification in 2d). HIV-1

155 also had no discernible effects on PB number or morphology in CFP-DCP1A biosensor
156 cells; with PB number being remarkable consistent and stable for all individual cells and
157 conditions (typically 6-9 PBs per cell, Fig. 2e with quantification in 2f). Based on these
158 largely negative results, we concluded that despite HIV-1's marked effects on YFP-A3G
159 as shown in Fig. 1, net modulation of PBs or induction of SGs are unlikely to be intrinsic
160 features of the HIV-1 replication cycle.

161 Because HIV-1 Gag was recently reported to inhibit SG formation[33,34], we also
162 tested the effects of treating HeLa.YFP-A3G or HeLa.YFP-TIA1 biosensor cells with Ars
163 at 31 hpi when NL4-3 Gag expression in HeLa cells is relatively high (*e.g.*, see [31]).
164 Contrary to our expectations, both YFP-A3G and YFP-TIA1 accumulated in SGs in Ars-
165 treated cells infected with either Vif+ or Vifxx viruses (Fig. 2g with quantification in 2h). To
166 localize Gag and genome under these conditions, we again performed combined Gag IF
167 and genome FISH, finding that the bulk of the HIV-1 genome signal co-localized with
168 YFP-A3G in Ars-induced SGs at this time point (Fig. 2i, *gag-pol* FISH). By contrast, the
169 cytoplasmic pool of Gag was largely excluded from these complexes (Fig. 2i, anti-p24).

170 SGs are induced in response to protein kinase R-mediated phosphorylation of
171 translation initiation factor eIF2a, triggering aggregation of scaffolding proteins that
172 include TIA1, TIAR, and G3BP1 in complex with mRNAs bound to translation initiation
173 factors and polysome-associated proteins [reviewed in [29,35]]. Accordingly, co-localization
174 of YFP-A3G with genomes in SGs could suggest stronger recognition of genomes by
175 YFP-A3G relative to Gag in association with free ribosomes in the cytosol.

176

177 **HIV-1 RNA genomes but not Gag modulate A3G subcellular mobility; evidence for**
178 **genome-A3G interactions in the cytosol.** So that we could also monitor Gag and
179 genome trafficking dynamics in living HeLa.YFP-A3G cells, we next engineered two-color,
180 HIV-1 genomes that encoded CFP-tagged Gag from a "self-tagging" genome bearing 24
181 copies of MS2 RNA binding loop (located in the *gag-pol* open reading frame; ORF) and
182 expressing an RFP-tagged MS2 bacteriophage (MS2-RFP) coat protein from the viral *nef*
183 locus (Gag-CFP/MS2-RFP virus, see cartoon depictions in Figs. 3a and 3c). Gag-CFP
184 allowed for single cell measurements of viral late gene expression, with genomes tracked
185 based on their binding to the MS2-RFP protein. Expression of Vif+ or Vifxx Gag-
186 CFP/MS2-RFP viruses recapitulated effects seen during infection with CFP reporter
187 viruses (Figs. 1 and 2); including rapid, Vif-dependent down-regulation of YFP-A3G
188 (decay rate = 25.9% per hour +/- 7.0%; n = 31, Fig. 3b, green, with quantification in Figs.
189 3e and 3f, Video 4) and, for Vif-deficient (Vifxx) conditions, co-clustering of YFP-A3G,
190 MS2-RFP-tagged genomes, and Gag-CFP to assembly sites at the plasma membrane
191 (Fig. 3d, arrows, Video 5; and see Fig. 4d for an image recorded at higher magnification).
192 We observed Vif-mediated YFP-A3G degradation to occur prior to the onset of virus
193 particle assembly (Fig. 3b, compare 2 h and 3 h time points), consistent with a prior
194 report[36], but at >1h after genomes had populated the cytoplasm (Fig. 3d, compare 1h and
195 4h time points).

196 Both prior to and during virus particle assembly, Vifxx genomes and YFP-A3G were
197 co-distributed in a non-localized fashion throughout the cytoplasm, with YFP-A3G but not
198 genome or Gag-CFP accumulating at PBs (Fig. 3d, 2 and 3 h time points post-detection
199 of MS2-RFP). To test if genomes and YFP-A3G were interacting in the fluid compartment,

200 we performed fluorescence recovery after photobleaching (FRAP) analysis to measure
201 rates of YFP-A3G recovery with or without genomes and in the presence or absence of
202 Gag (Figs. 3g, 3h, and quantification in 3i). Infection with Vifxx HIV-1 mCherry reporter
203 virus reduced rates of YFP-A3G recovery ($t_{1/2}$ = 34.4 s +/- 5.3 s; *n*=8) relative to an
204 uninfected "YFP-A3G alone" control ($t_{1/2}$ = 27.0 s +/- 13.5 s; *n*=14). Interestingly, we also
205 observed incomplete recovery of YFP-A3G at the latest time points in infected cells (~75%
206 recovery compared to nearly 90% for untreated control cells Fig. 3i); suggesting virus-
207 induced immobilization of YFP-A3G [37].

208 Expression of genomes in the absence of Gag using a "genome only" Vifxx MS2-
209 RFP genome, wherein we mutated the *gag* start codon to abolish Gag synthesis (see Fig.
210 3g), yielded markedly slower rates of YFP-A3G recovery ($t_{1/2}$ = 70.8 s +/- 27.6 s; *n*=6)
211 relative to both the "YFP-A3G Alone" condition, and a "Gag Only" condition wherein we
212 expressed Gag-mCherry from an mRNA modified to lack 5' and 3' viral regulatory RNA
213 sequences and codon-optimized to further reduce potential contributions of viral *cis*-
214 acting RNA elements located in the *gag* ORF (COGag-mCh; $t_{1/2}$ = 30 s +/- 8.9 s; *n*=7)
215 (Fig. 3i). Taken together, because the expression of genomes but not Gag altered YFP-
216 A3G movements in the cytoplasm based on FRAP analysis, genome-YFP-A3G
217 interactions are likely initiated in the cytoplasm independently of virus particle assembly;
218 and potentially even prior to the onset of Gag synthesis.

219

220 **Genome-A3G interactions are selective, Gag-independent, and initiated prior to the**
221 **onset of virus particle assembly.** Because FRAP was unable to distinguish between
222 direct or indirect genome-A3G interactions, we next developed a single cell assay to allow

223 us to measure the strength and specificity of RNA-RBP interactions in the cytoplasm head
224 on; dubbed the In-Cell RNA-Protein Interaction Protocol (IC-IP) (depicted in Fig. 4a). The
225 IC-IP was based on the principle of immobilizing genomes at unnatural sites in the
226 cytoplasm (*e.g.*, membranes or the actin cytoskeleton) using an MS2-based tethering
227 strategy that we have described previously[38]. Should an RBP such as YFP-A3G be
228 strongly associated with the tethered genome, its localization will be also shifted with clear
229 evidence of RNA-RBP co-localization at the unnatural site of tethering.

230 For genome-A3G IC-IPs, MSL-bearing genomes served as bait for YFP-A3G, as
231 depicted in Fig. 4a. Genome retargeting was achieved by co-expressing "targeter" MS2
232 coat proteins that were modified to tether MSL-tagged genomes to either membranes
233 (using Src-MS2; bearing a 10 amino-acid membrane targeting signal) or the actin
234 cytoskeleton (using Lifeact-MS2; bearing a 17 amino acid F-actin targeting signal) (Fig.
235 4b). The Src-MS2 and Lifeact-MS2 targeters were fused to iRFP670 so that we could co-
236 visualize both the targeter and the genome (labelled with the self-tagging MS2-RFP
237 "tracker" protein, see cartoon depiction in Fig. 4c) without experiencing spectral overlap
238 (see Fig. 4d).

239 Co-expression of two-color Vifxx Gag-CFP/MS2-RFP genomes with the Src-MS2-
240 iRFP or Lifeact-MS2-iRFP targeters caused moderate re-localization of Gag-CFP
241 proteins from the cytosolic pool to intracellular vesicles (Fig. 4d, compare panels iv. and
242 ix.) or F-actin filaments (Fig. 4d, compare panels iv. to xiv.), respectively; consistent with
243 a subset of Gag proteins co-trafficking with its genome substrate in the cytosol (as we
244 have previously shown[38]). Remarkably, however, re-localization of YFP-A3G was more
245 striking, with >50% of the net YFP-A3G per cell fluorescent signal now associated with

246 intracellular vesicles or F-actin filaments (Fig. 4d, compare panels ii., viii., and xiii., and
247 see YFP-A3G regions-of-interest; ROI; with quantification in 4e and 4f). Consistent with
248 our results from FRAP analyses (Figs. 3g and 3h), a “genome only” bait was sufficient to
249 recruit >50% of YFP-A3G to intracellular vesicles as directed by Src-MS2, suggesting that
250 Gag plays no role in genome-A3G cytosolic interactions (Figs. 5a and 5b). By contrast, a
251 control MSL-bearing mRNA encoding codon-optimized Gag-CFP (“Gag Only”) had no
252 effect on YFP-A3G cytoplasmic distribution (Figs. 5c and 5d). Collectively, these results
253 indicated that HIV-1 genome-A3G interactions in the cytoplasm are strong, specific, and
254 occur in the presence or absence of Gag.

255 A particularly useful feature of the IC-IP is that it could be coupled to video
256 microscopy in order to determine the timing of YFP-A3G-genome interactions timed to
257 the onset of viral gene expression. Live cell imaging of cells co-expressing Src-MS2-
258 iRFP670 with a “Genome Only” RNA bait demonstrated that YFP-A3G was relocalized to
259 vesicles within two hours of first detecting genome expression in the cytoplasm (Fig. 5e,
260 compare 1h and 2h time points, and see Video 6 for additional detail). Accordingly, this
261 experiment indicated that strong genome-A3G interactions are initiated concomitantly
262 with or very soon after genome nuclear export.

263

264 **Tethering A3G to membranes arrests HIV-1 genome trafficking and reduces virus**
265 **particle production.** We reasoned that if A3G’s interactions with genomes were
266 sufficiently strong, then tethering A3G to membranes would, as a corollary, arrest HIV-1
267 genome mobility in the cytosol and abolish genome trafficking to sites of virus particle
268 assembly. To test this idea, we engineered a “reciprocal” IC-IP experiment (Fig. 6a)

269 wherein YFP-A3G was modified so that it would bind membranes due to its bearing the
270 same N-terminal Src-derived myristoylation signal we used for our Src-MS2 genome
271 retargeting constructs (Figs. 2b-2e). This fusion protein (Src-YFP-A3G) was co-
272 expressed with two-color (Gag-CFP/MS2-RFP) Vifxx (Fig. 6b) or a CFP-tagged variant
273 (Src-CFP-A3G) co-expressed with one-color (MS2-RFP) "Genome Only" Vifxx genomes
274 (Fig. 6c). As would be anticipated for a strong interaction, Src-FP-A3G expression
275 induced the marked clustering of MS2-RFP-tagged genomes to perinuclear vesicles, with
276 genomes co-localizing with Src-FP-A3G (Figs. 6b and 6c). To address the more relevant
277 scenario of infected cells, we also generated a cell line constitutively expressing Src-YFP-
278 A3G (HeLa.Src-YFP-A3G cells) and infected these cells with a Vifxx reporter virus (Fig.
279 6d). As expected, we observed genomes (and, to a lesser extent, Gag) co-clustering with
280 Src-YFP-A3G at cytoplasmic vesicles at 24 hpi, detected using combined IF/FISH (Fig.
281 6d, bottom, white arrows).
282 We hypothesized that arrest of genome subcellular trafficking due to Src-YFP-A3G
283 expression would reduce Gag synthesis and net virus particle production. Consistent with
284 this hypothesis, co-expression of Src-YFP-A3G or a Src-MS2 control with MSL-tagged 2-
285 color genome (Gag-BFP in this experiment) yielded a dose-dependent reduction to
286 cytosolic Gag level and net efficiency of virus particle release (Fig. 6e). Taken together,
287 these experiments indicated that A3G-genome interactions in the cytosol are sufficiently
288 strong that tethering A3G to membranes can effectively repurpose this protein as an
289 inhibitor of genome trafficking and net virion production.
290

291 **The presence of genomes promotes more consistent per virion delivery of A3G to**
292 **sites of virus particle assembly.** Combined, the above experiments suggested that
293 A3G has evolved to preferentially recognize one or more HIV-1 genome RNA signatures.
294 However, A3G is encapsidated by Gag into virus particles even in the absence of
295 packageable genomes[17–19]. In an effort to better rationalize prior observations of A3G
296 genome specificity vs. promiscuity, we performed a comparative single virion analysis
297 (SVA) of A3G delivery into virus particles; based on a technique originally pioneered by
298 the Hu and Pathak groups wherein fluorescently-labeled virus-like particles (VLPs) are
299 harvested from HEK293T cells (that produce a greater quantity of particles relative to
300 HeLa) and subjected to sub-micron quantitative multicolor fluorescence imaging to
301 measure relative levels of per particle genome and/or A3G incorporation[39,40] (Fig. 7). For
302 our analysis, we compared per particle levels of YFP-A3G encapsidation for four
303 independent Gag/genome scenarios (depicted in Fig. 7a); "Gag-Only" mRNAs encoding
304 codon-optimized Gag-CFP (COGag-CFP = "Gag-Only"), viral Vif+ or Vifxx 2-color HIV
305 Gag-CFP/MS2-RFP genomes, or mRNAs encoding codon-optimized Gag-CFP wherein
306 the NC RNA-binding domain was replaced by a leucine zipper (ΔNCzip) to abolish Gag-
307 RNA binding (based on [41]). As expected, YFP-A3G packaging was only observed for
308 COGag and the Vifxx HIV-1 conditions (Fig. 7b).
309 Using SVA, Vif+ and Vifxx viruses exhibited high efficiency MS2-RFP incorporation
310 (~89 and ~88% of Gag-CFP particles scoring positive for MS2-RFP, respectively), very
311 consistent with a prior report of HIV-1 genome packaging efficiency[39]. Vifxx Gag-
312 CFP/MS2-RFP particles exhibited a similar frequency of YFP-A3G incorporation (86% of
313 total Gag-CFP particles) (Fig. 7c and quantification in 7d). However, for "Gag-Only"

314 (COGag-CFP) particles, the frequency of detectable YFP-A3G incorporation was lower
315 (57% efficiency), intermediate to Vifxx HIV-1 vs. the ΔNCzip “no-RNA” negative control
316 (Fig. 7c and quantification in 7d). COGag particles also exhibited reduced per virion levels
317 of YFP-A3G fluorescence when compared to full-length, Vifxx HIV (Fig. 7c and
318 quantification in 7e). In sum, these data indicated that, although genomes are not
319 essential for YFP-A3G delivery to virus particles, selective genome-A3G interactions
320 promote a more consistent and more enriched per virion delivery of A3G to virus particle
321 assembly sites.

322 **DISCUSSION**

323 Herein we studied the HIV-1 life cycle from the host cell perspective, combining
324 several complementary live cell imaging approaches with functional assays to
325 characterize the coordinated behaviors A3G, PB or SG proteins, and viral elements (Gag
326 and genome) over an entire round of viral replication (summarized in Fig. S1).

327 Our YFP-A3G biosensor allowed for indirect measurements of HIV-1 replication
328 kinetics in single cells and exposed A3G behaviors including; (1) that Vif-mediated A3G
329 degradation occurs from all subcellular pools simultaneously (Fig. 1d and Movie 1); (2)
330 that A3G suppression by Vif is remarkably stable and maintained over the entire late
331 phase of infection (lasting hours to days, see Figs. 1d, Movie 1, and 1e); and (3) that A3G
332 degradation is completed prior to the onset of virus particle assembly (very consistent
333 with prior report from Holmes *et al*.,[36] but shown here to be after genome nuclear export)
334 (Fig. 3b). In the absence of Vif, we could also monitor virus particle assembly, observing
335 large quantities of YFP-A3G being re-localized from the cytoplasm to the plasma
336 membrane during this process (Fig. 1f and Video 2). Taken together, on a technical level
337 there should be great utility in the general strategy of tracking RBP biosensors to detect
338 virus replication dynamics and study host cell responses (*e.g.*, see also RVA16-induced
339 stress in Fig. 2b). Moreover, now validated, HeLa.YFP-A3G cells should serve as useful
340 multivariate reporter system for further dissection of the viral and host machineries
341 governing A3G degradation and packaging.

342 Despite HIV-1's marked effects on YFP-A3G behaviors, we observed little to no
343 discernible effects of HIV-1 on SGs or PBs monitored using our YFP-TIA1 or CFP-DCP1A
344 biosensors, with or without Vif expression (Fig. 2). These movies reinforce that

345 modulation of PB number or architecture or SG induction is unlikely to be an intrinsic
346 feature of the HIV-1 life cycle[27,28]. Overall, the underlying significance of A3G's localization
347 to PBs and SGs remains is unknown; but predicted to spatially coupled A3G to RNP
348 complexes with active roles in viral mRNA surveillance (*i.e.*, PBs are sites miRNA-
349 dependent mRNA decay and SGs can suppress viral translation)[23,24,26]. In this context,
350 we speculate that all successful retroviruses and endogenous elements must adapt to
351 subvert, suppress, or avoid PB- or SG-associated activities. Indeed, HIV-1[42,43], other
352 retroviruses[44,45], and endogenous retroelements including LINEs[46] and yeast Ty
353 elements[47] are thought to exploit non-membranous RNP complexes related to PBs/SGs
354 in order to compartmentalize activities including mRNA translation and genome
355 packaging. Regarding suppression, intriguing recent work from Mouland and colleagues
356 has shown HIV-1 to actively inhibit SG formation, proposed to reduce the potential for
357 stress signaling triggered by Gag NC interacting with host RNA species[33,34]. While we did
358 not observe overt SG suppression in this study (Figs. 2g-i), the dynamics of this process
359 warrant additional investigation and it seems reasonable to posit that retroviruses prevent
360 SG formation to promote a fluid flow of genomes from the nucleus to polysomes and then
361 on to capsid assembly sites. Overall, however, our data support the notion that HIV-1's
362 general *modus operandi* is to largely avoid association with visible PBs or induction of
363 SGs.

364 At a more molecular level, our imaging assays also suggest that A3G is able to
365 selectively compete for genome binding in the cytosol. First, HIV-1 genomes but not Gag
366 rapidly accumulated at YFP-A3G-enriched SGs in infected cells after Ars treatment (Fig
367 2i). Second, based on FRAP analysis, the presence of genomes, but not Gag, reduces

368 A3G mobility in the cytoplasm (Fig. 3g and 3h). Third, and most convincingly, our IC-IP
369 experiments demonstrated that >50% of the cytosolic YFP-A3G is recruited to
370 membranes or F-actin by Src- or Lifeact-MS2-tethered genomes, respectively, (Fig. 4f);
371 effects that were far less evident for Gag-CFP; not observed in the absence of genomes
372 (Fig. 5d); and detected soon if not immediately after genome nuclear export (Fig. 5e). As
373 to *why* A3G competes for genome binding, single virion analyses (Fig. 7) revealed an
374 ~90% frequency of A3G incorporation into genome-containing virions relative to "Gag-
375 only" particles wherein the frequency of A3G incorporation was less than 60%. This result
376 suggests to us that, although A3G-RNA binding is, overall, relatively promiscuous[19], it has
377 evolved to preferentially target genomes in a way that ensures consistent and efficient
378 delivery to virions, largely consistent with a model recently proposed by Bieniasz and
379 colleagues wherein Gag and A3G are adapted to compete for similar RNA sequences[20].
380 In this way, A3G maximizes its antiviral potential and thus necessitated evolution of the
381 Vif antagonist. Endeavors to further delineate the relevant protein constituents of A3G-
382 genome "surveillance" complexes, and to determine whether or not A3G exhibits
383 differential detection of genomes destined for packaging vs. translation (as *gag-pol*
384 mRNAs), are ongoing.

385 To summarize, our studies reinforce that the core, essential nature of genome
386 trafficking in the cytosol is diffusion in dynamic association with RNP complexes, with
387 some proteins (*e.g.*, A3G) more strongly associated with genomes than others. While we
388 have yet to define the RNA signature(s) that specify genome detection by A3G, our
389 observations may be informative in the context of recent CLIP-seq studies demonstrating
390 A3G's RNA-binding preference to be relatively sequence non-specific[19,20] coupled to

391 compelling recent work showing that HIV-1 genomes are selectively enriched in selective
392 post-transcriptional regulatory marks including $N_6$ methyladenosine (m6a)[48–50], 5-
393 methylcytosine (m5c), and 2'O-methylation[51]. Artificially tethering A3G to membranes
394 restricts HIV-1 genome trafficking and virus particle assembly (Fig. 6). Based on these
395 effects, we predict it will be feasible to design inhibitory molecules or biologicals capable
396 of achieving similar strong, selective inhibition of HIV-1 RNA trafficking, translation, and
397 genome packaging in the context of antiviral strategies.

**ACKNOWLEDGEMENTS**

We thank Randall Massey at the University of Wisconsin SMPH Electron Microscopy Facility for assistance with EM sample preparation. We are grateful to Michael Malim (King's College London), Chad Swanson, (King's College London), and Sarah Gallois-Montbrun (Institut Cochin) for plasmid reagents and advice. The following reagent was obtained through the NIH AIDS Reagent Program, Division of AIDS, NIAID, NIH: HIV-1 p24 hybridoma (183-H12-5C) (from Bruce Chesebro)[52]. We thank Kelly Watters, Marchel Hill, and Ann Palmenberg for RVA16[32]. This study was supported by NIH grants RO1AI110221 and U54AI150470; the Wisconsin Partnership Program New Investigator Program (ID 2830); the Greater Milwaukee Foundation's Shaw Scientist Program; and the UW-Madison UW2020 Program to N.M.S. J.T.B. was supported by National Science Foundation Graduate Research Fellow Program grant DGE-1256259 and both a Research Competition Award and a Dissertation Completion Fellowship from the UW—Madison office of the Vice Chancellor of Research and Graduate Education. Any opinions, findings, and conclusions or recommendations expressed in this material are those of the authors and do not necessarily reflect the views of the National Science Foundation. E.L.E. III received support from NIH training grant CA009135 and an Advance Opportunity Fellowship from the UW-Madison SciMed/GRS program. B.E.B. was supported by National Science Foundation Graduate Research Fellow Program grant DGE-1256259 and NIH training grant GM008349. S.L.F. received support from a UW-Madison Hilldale Undergraduate Research Fellowship.

**AUTHOR CONTRIBUTIONS:**

JTB and NMS conceived the project, designed reagents, and established methods. JTB carried out all experiments and wrote the first version of the manuscript. ELE, BEB, SLF, LES, and AEB contributed reagents and generated preliminary data. JTB, ELE, and NMS processed and analyzed data. All authors contributed to the final revised manuscript and approved submission.

426 **METHODS**

427 **Cell culture, plasmids, and stable cell lines.** Human HeLa and HEK293T cell lines
428 (obtained from ATCC) were cultured in DMEM (Sigma-Aldrich) supplemented with 10%
429 fetal bovine serum (heat-inactivated, filter-sterilized), 1% L-glutamine, and 1% penicillin-
430 streptomycin. HeLa.YFP-A3G, HEK293T.YFP-A3G, HeLa.Src-YFP-A3G, HeLa.YFP-
431 TIA1, and HeLa.CFP-DCP1a were generated as previously described[38]. Briefly, YFP-
432 A3G, Src-YFP-A3G, YFP-TIA1, and CFP-DCP1a cDNA[24] were inserted into a MIGR1-
433 derived retroviral vector (pCMS28) upstream of sequence encoding an internal ribosome
434 entry site (IRES) and a second reading frame encoding Puromycin-N-acetyltransferase[48].
435 High performance clones were selected by limiting dilution and maintained in 2μg/mL
436 puromycin. YFP, YFP-A3G, and Src-YFP-A3G as well as CFP versions of construct were
437 also generated using the pcDNA3.1 transient expression vector backbone. HIV-1 reporter
438 virus plasmids were derived from the pNL4-3 molecular clone[53] bearing inactivating
439 mutations in *env*, *vpr*, and expressing a green fluorescent protein (GFP) reporter from the
440 *nef* locus (E-R-/GFP)[54]; with the GFP reporter replaced with either cerulean fluorescent
441 protein (CFP) or mCherry (mCh). Vif-minus HIV-1 reporter virus plasmids (Vifxx CFP and
442 Vifxx mCherry) were generated by changing *vif* codons 26 and 27 to stop codons[55] using
443 overlapping PCR and inserted into Vif+ CFP and Vif+ mCherry plasmids. Two-color
444 fluorescent HIV-1 reporter viruses (Gag-CFP/MS2-RFP) were generated by replacing the
445 *gag* reading frame in Vif+ and Vifxx CFP reporter viruses with *gag-CFP* just upstream of
446 a cassette encoding 24 copies of the MS2 bacteriophage RNA stem loop (MSL, a kind
447 gift of Robert Singer, Albert Einstein University, New York, NY, USA)[56], and then
448 subsequently replacing CFP with sequence encoding the MS2 coat protein fused to

449 mApple or mCherry and bearing an SV40 nuclear localization signal (MS2-RFP). Gag
450 was also fused to mTagBFP2 for select experiments (*e.g.*, Fig. 6e) in order to avoid
451 CFP/YFP cross-detection when immunoblotting for Src-YFP-A3G. Mutated versions of
452 full-length HIV-1 were generated using overlapping PCR as previously described[38]. Src-
453 MS2-CFP, Src-MS2-RFP, and Src-MS2-iRFP targeting constructs encoding an amino-
454 terminal membrane targeting signal derived from the Src kinase (MGSSKSKPKD) were
455 generated by overlapping PCR and subcloned into pcDNA3.1. mTurquoise2 (CFP) and
456 mApple (RFP) were gifts of Michael Davidson (Addgene # 54843 and 54747,
457 respectively). iRFP670 cDNA[57] was amplified from the ColorfulCell expression plasmid,
458 a gift of Pierre Neveu (Addgene plasmid # 62449)[58]. mTagBFP2[59] was a gift of Michal
459 Davidson (Addgene plasmid # 55302).
460
461 **Retroviral assembly and infectivity assays**. Cells at 30-40% confluency were
462 transfected with 2µg DNA in six well plates using polyethylenimine (PEI; #23966,
463 Polysciences Inc.). pcDNA3.1 or pBlueScript were used as empty vector controls. Culture
464 media were replaced at 24 hours post-transfection and cell lysates and supernatants were
465 harvested for immunoblot analysis at 48 hours as previously described[60](Sherer et al.
466 2011). Briefly, 1mL of harvested culture supernatant was filtered, underlaid with 20%
467 sucrose (w/v) in PBS, subjected to centrifugation at >21,000g for two hours at 4ºC, and
468 viral pellets were resuspended in 35µL dissociation buffer (62.5 mM Tris-HCl, pH 6.8,
469 10% glycerol, 2% sodium dodecyl sulfate [SDS], 5% β-mercaptoethanol). Cells were
470 harvested in 500µL radioimmunoprecipitation assay (RIPA) lysis buffer (10 mM Tris-HCl,
471 pH 7.5, 150 mM NaCl, 1 mM EDTA, 0.1% SDS, 1% Triton X-100, 1% sodium

472 deoxycholate), homogenized by passage through a 26G needle, subjected to
473 centrifugation at 1,500g for 20 minutes at 4ºC, and liquid supernatant fraction was
474 combined 1:1 with 2X dissociation buffer. Proteins were resolved by sodium dodecyl
475 sulfate-polyacrylamide gel electrophoresis (SDS-PAGE) and transferred to 0.2 µm
476 nitrocellulose membranes. Gag was detected using a mouse monoclonal antibody
477 recognizing HIV-1 capsid/p24 (183-H12-5C; 1:1000 dilution) from Dr. Bruce Chesebro
478 and obtained from the NIH AIDS Research and Reference Reagent Program (Bethesda,
479 MD, USA)[52] and anti-mouse secondary antibodies conjugated to an infrared fluorophore
480 (IRDye680LT, 1:10000 dilution, Li-Cor Biosciences) for quantitative immunoblotting. As
481 loading controls, heat shock protein 90A/B (HSP90) was detected using a rabbit
482 polyclonal antibody (H-114, 1:2500 dilution, Santa Cruz Biotechnology, Santa Cruz, CA,
483 USA) or glyceraldehyde 3-phosphate dehydrogenase (GAPDH) was detected using a
484 mouse monoclonal antibody (6C5, 1:2500 dilution, Santa Cruz Biotechnology) and anti-
485 rabbit or anti-mouse secondary secondary antibodies conjugated to an infrared
486 fluorophore (IRDye800CW, 1:7500 dilution, Li-Cor Biosciences). YFP-containing proteins
487 (*e.g.*, YFP-A3G) were detected using a rabbit polyclonal antibody recognizing GFP (FL
488 sc-8334, 1:1000 dilution, Santa Cruz Biotechnology) and anti-rabbit secondary antibodies
489 conjugated to an infrared fluorophore (IRDye800CW). For infectivity assays,
490 supernatants containing single-round infectious HIV-1 virions (pseudo-typed with VSV-G)
491 were filtered and then added to target HeLa cells in the presence of 10µg/mL polybrene.
492 Approximately 36 hours later, target HeLa cells were scanned using a BioTek Cytation5
493 to detect reporter CFP (455nm/510nm excitation/emission filter) expression following
494 infection.

495

496 **Microscopy, immunofluorescence, and FISH.** Cells were plated in 24-well glass-
497 bottom plates (Eppendorf) or 8-well microslides (IBIDI) and transfected using PEI or
498 infected with HIV-1 reporter viruses. Transfection mixes contained 1µg (24-well) or 333ng
499 (IBIDI) total plasmid DNA, respectively. Infections were performed with VSV-G pseudo-
500 typed HIV-1 reporter viruses produced in HEK293T cells and titered on HeLa cells to
501 determine MOI of 0.5-1, thereby ensuring that 33-66% of the cells would be infected per
502 experiment. Fixed-cell experiments were performed on a Nikon Ti-Eclipse inverted wide-
503 field microscope (Nikon Corporation, Melville, NY, USA) using a 100x Plan Apo oil
504 objective (numerical aperture [NA], 1.45). Transfected cells were fixed 24 – 32 hours post-
505 transfection and infected cells were fixed 42 hours post-infection using 4%
506 paraformaldehyde. If treated with 250 µM sodium arsenite (Sigma-Aldrich), drug or an
507 equivalent volume of dimethyl sulfoxide were added to cell culture wells at approximately
508 one hour prior to fixation and returned to incubation at 37ºC. Live-cell imaging
509 experiments were also performed on a Nikon Ti-Eclipse inverted wide-field microscope
510 using a 20x Plan Apo objective lens (NA, 0.75) with images acquired every 60 minutes
511 (except where otherwise indicated) over a time course of 16 to 90 hours. Images were
512 acquired using an ORCA-Flash4.0 CMOS camera (Hammatsu Photonics) and the
513 following excitation/emission filter sets (nanometer ranges): BFP (402/455), CFP
514 (430/470), YFP (510/535), mApple (555/605), mCherry (572/632), and iRFP (645/705).
515 All images were processed and analyzed using FIJI/ImageJ2.

516 For fixed-cell experiments using FISH, cells were plated as described as above
517 and previously[38]. At 42 hours post-infection or after 24 hours plated (for uninfected cells),

518 cells were washed, fixed in 4% formaldehyde, and permeabilized in 70% ethanol for at
519 least 4 hours at 4ºC. Custom Stellaris FISH probes were designed to recognize NL4-3
520 HIV-1 *gag-pol* reading frame nucleotides 386-4456 using the Stellaris RNA FISH Probe
521 Designer 4.1 (Biosearch Technologies, Inc.) available online. To detect *yfp* mRNAs, we
522 used a DesignReady Probe set specific to eGFP. Both probe sets were labeled with CAL
523 Fluor Red 590 Dye (Biosearch Technologies, Inc.). Samples were hybridized with the
524 *gag/gag-pol* probe set according to the manufacturer's instructions available online.
525 Simultaneous immunofluorescence to detect Gag used a mouse monoclonal antibody
526 specific to p24 (#24-2, a gift from Dr. Michael Malim). Imaging experiments were
527 performed as describe above on a Nikon Ti-Eclipse inverted wide-field microscope using
528 a 100x Plan Apo objective lens.

529 FRAP experiments were performed using a Nikon Ti-Eclipse inverted A1R+
530 resonant/galvano hybrid confocal line-scanning microscope. Images were captured using
531 a 20x Plan Apo objective lens (NA, 0.75) and a GaAsP multi-detector for 488 and 560nm
532 channels. YFP-A3G was imaged using the 488nm laser at a low arbitrary intensity and
533 photobleached using the laser's maximum intensity. MS2-RFP and COGag-mCherry
534 were imaged using the 560nm laser at a low arbitrary intensity. Cells were maintained in
535 an environmental chamber (Pathology Devices, Inc.) at 37ºC, 5% $CO_2$, and 50% humidity.
536 Cells were imaged every 30 seconds for 4 frames prior to photobleaching (3 rapid
537 ablations of cytoplasmic ROIs 10μm in diameter) followed by imaging every 5 seconds
538 for a minute, 15 seconds for four minutes, and 30 seconds for 5 minutes. This time frame
539 was sufficient for fluorescence recovery to reach a plateau. FRAP analysis was performed

540 using the FIJI plugin FRAP Profiler[61] that adjusts for incidental field photobleaching
541 outside the ROI.
542 Single virion analyses (SVA) were performed as previously described[39]. Virus
543 particles were produced as described above for western blotting in HEK293T.YFP-A3G
544 cells to maintain consistent levels of YFP-A3G. Filtered culture supernatants (750µL)
545 were purified by sucrose centrifugation as described above and resuspended in 100µL
546 1x PBS (Sigma-Aldrich). 24-well plates were pre-coated with 2% FBS diluted in 1x PBS
547 for at least 30 minutes, this solution was removed, and the resuspended concentrated
548 virus particles were added to wells. Images were acquired on a Nikon Ti-Eclipse inverted
549 wide-field microscope using a 100x Plan Apo objective lens (NA, 1.45). These images
550 were processed and analyzed using Analyze Particles plugin in FIJI/ImageJ2[62].
551
552 **Thin-section electron microscopy.** HeLa.YFP-A3G were infected with Vif+ CFP or
553 Vifxx CFP HIV-1 viruses and fixed at 48 hours for chemical processing as previously
554 described[63]. Samples were sectioned into 100nm slices and with sections collected on
555 copper thin-bar grids. Sections were observed with a Phillips CM120 transmission
556 electron microscope, and images were collected with a MegaView III (Olympus-SIS,
557 Lakewood, CO, USA) side-mounted digital camera. All images were processed and
558 analyzed using FIJI/ImageJ2[62].
559
560 **Statistics.** For assembly assays (Figs. 1b and 6e), results were obtained from three
561 biological replicates as defined as cells plated in six well plates transfected and processed
562 on separate days. Graphs plot the mean value with error bars representing the standard

deviation of the mean with the exception of Fig. 7e, a violin plot showing all data points with the mean (solid line) and quartiles (dashed lines) indicated. All statistical comparisons were carried out using the two-tailed Student's *t* test and performed using Microsoft Excel or Graphpad Prism.

567 **REFERENCES**


568 1. Bolinger, C. & Boris-Lawrie, K. Mechanisms employed by retroviruses to exploit host
569 factors for translational control of a complicated proteome. *Retrovirology* **6**, 8 (2009).
570 2. Cochrane, A. W., McNally, M. T. & Mouland, A. J. The retrovirus RNA trafficking
571 granule: from birth to maturity. *Retrovirology* **3**, 18 (2006).
572 3. Karn, J. & Stoltzfus, C. M. Transcriptional and posttranscriptional regulation of HIV-1
573 gene expression. *Cold Spring Harb. Perspect. Med.* **2**, a006916 (2012).
574 4. Swanson, C. M. & Malim, M. H. Retrovirus RNA trafficking: from chromatin to
575 invasive genomes. *Traffic Cph. Den.* **7**, 1440–1450 (2006).
576 5. Harris, R. S. *et al.* DNA deamination mediates innate immunity to retroviral infection.
577 *Cell* **113**, 803–809 (2003).
578 6. Malim, M. H. APOBEC proteins and intrinsic resistance to HIV-1 infection. *Philos.*
579 *Trans. R. Soc. Lond. B. Biol. Sci.* **364**, 675–687 (2009).
580 7. Refsland, E. W. & Harris, R. S. The APOBEC3 family of retroelement restriction
581 factors. *Curr. Top. Microbiol. Immunol.* **371**, 1–27 (2013).
582 8. Sheehy, A. M., Gaddis, N. C., Choi, J. D. & Malim, M. H. Isolation of a human gene
583 that inhibits HIV-1 infection and is suppressed by the viral Vif protein. *Nature* **418**,
584 646–650 (2002).
585 9. Mariani, R. *et al.* Species-specific exclusion of APOBEC3G from HIV-1 virions by Vif.
586 *Cell* **114**, 21–31 (2003).
587 10. Sheehy, A. M., Gaddis, N. C. & Malim, M. H. The antiretroviral enzyme APOBEC3G
588 is degraded by the proteasome in response to HIV-1 Vif. *Nat. Med.* **9**, 1404–1407
589 (2003).
590 11. Stopak, K., de Noronha, C., Yonemoto, W. & Greene, W. C. HIV-1 Vif blocks the
591 antiviral activity of APOBEC3G by impairing both its translation and intracellular
592 stability. *Mol. Cell* **12**, 591–601 (2003).
593 12. Freed, E. O. HIV-1 assembly, release and maturation. *Nat. Rev. Microbiol.* **13**, 484–
594 496 (2015).
595 13. Eckwahl, M. J. *et al.* Analysis of the human immunodeficiency virus-1 RNA
596 packageome. *RNA N. Y. N* **22**, 1228–1238 (2016).
597 14. Rulli, S. J. *et al.* Selective and nonselective packaging of cellular RNAs in retrovirus
598 particles. *J. Virol.* **81**, 6623–6631 (2007).
599 15. Zennou, V., Perez-Caballero, D., Göttlinger, H. & Bieniasz, P. D. APOBEC3G
600 incorporation into human immunodeficiency virus type 1 particles. *J. Virol.* **78**,
601 12058–12061 (2004).
602 16. Khan, M. A. *et al.* Analysis of the contribution of cellular and viral RNA to the
603 packaging of APOBEC3G into HIV-1 virions. *Retrovirology* **4**, 48 (2007).
604 17. Cen, S. *et al.* The interaction between HIV-1 Gag and APOBEC3G. *J. Biol. Chem.*
605 **279**, 33177–33184 (2004).
606 18. Alce, T. M. & Popik, W. APOBEC3G is incorporated into virus-like particles by a
607 direct interaction with HIV-1 Gag nucleocapsid protein. *J. Biol. Chem.* **279**, 34083–
608 34086 (2004).
609 19. Apolonia, L. *et al.* Promiscuous RNA binding ensures effective encapsidation of
610 APOBEC3 proteins by HIV-1. *PLoS Pathog.* **11**, e1004609 (2015).
611 20. York, A., Kutluay, S. B., Errando, M. & Bieniasz, P. D. The RNA Binding Specificity

612 of Human APOBEC3 Proteins Resembles That of HIV-1 Nucleocapsid. *PLoS*
613 *Pathog.* **12**, e1005833 (2016).
614 21. Svarovskaia, E. S. *et al.* Human apolipoprotein B mRNA-editing enzyme-catalytic
615 polypeptide-like 3G (APOBEC3G) is incorporated into HIV-1 virions through
616 interactions with viral and nonviral RNAs. *J. Biol. Chem.* **279**, 35822–35828 (2004).
617 22. Gallois-Montbrun, S. *et al.* Comparison of cellular ribonucleoprotein complexes
618 associated with the APOBEC3F and APOBEC3G antiviral proteins. *J. Virol.* **82**,
619 5636–5642 (2008).
620 23. Wichroski, M. J., Robb, G. B. & Rana, T. M. Human retroviral host restriction factors
621 APOBEC3G and APOBEC3F localize to mRNA processing bodies. *PLoS Pathog.* **2**,
622 e41 (2006).
623 24. Gallois-Montbrun, S. *et al.* Antiviral protein APOBEC3G localizes to
624 ribonucleoprotein complexes found in P bodies and stress granules. *J. Virol.* **81**,
625 2165–2178 (2007).
626 25. Chable-Bessia, C. *et al.* Suppression of HIV-1 replication by microRNA effectors.
627 *Retrovirology* **6**, 26 (2009).
628 26. Nathans, R. *et al.* Cellular microRNA and P bodies modulate host-HIV-1 interactions.
629 *Mol. Cell* **34**, 696–709 (2009).
630 27. Izumi, T. *et al.* Mov10 and APOBEC3G localization to processing bodies is not
631 required for virion incorporation and antiviral activity. *J. Virol.* **87**, 11047–11062
632 (2013).
633 28. Phalora, P. K., Sherer, N. M., Wolinsky, S. M., Swanson, C. M. & Malim, M. H. HIV-1
634 replication and APOBEC3 antiviral activity are not regulated by P bodies. *J. Virol.* **86**,
635 11712–11724 (2012).
636 29. Ivanov, P., Kedersha, N. & Anderson, P. Stress Granules and Processing Bodies in
637 Translational Control. *Cold Spring Harb. Perspect. Biol.* **11**, (2019).
638 30. Kedersha, N. *et al.* Dynamic shuttling of TIA-1 accompanies the recruitment of
639 mRNA to mammalian stress granules. *J. Cell Biol.* **151**, 1257–1268 (2000).
640 31. Evans, E. L., Becker, J. T., Fricke, S. L., Patel, K. & Sherer, N. M. HIV-1 Vif's
641 Capacity To Manipulate the Cell Cycle Is Species Specific. *J. Virol.* **92**, (2018).
642 32. Watters, K. *et al.* Differential Disruption of Nucleocytoplasmic Trafficking Pathways
643 by Rhinovirus 2A Proteases. *J. Virol.* **91**, (2017).
644 33. Cinti, A., Le Sage, V., Ghanem, M. & Mouland, A. J. HIV-1 Gag Blocks Selenite-
645 Induced Stress Granule Assembly by Altering the mRNA Cap-Binding Complex.
646 *mBio* **7**, e00329 (2016).
647 34. Valiente-Echeverría, F. *et al.* eEF2 and Ras-GAP SH3 domain-binding protein
648 (G3BP1) modulate stress granule assembly during HIV-1 infection. *Nat. Commun.* **5**,
649 4819 (2014).
650 35. Protter, D. S. W. & Parker, R. Principles and Properties of Stress Granules. *Trends*
651 *Cell Biol.* **26**, 668–679 (2016).
652 36. Holmes, M., Zhang, F. & Bieniasz, P. D. Single-Cell and Single-Cycle Analysis of
653 HIV-1 Replication. *PLoS Pathog.* **11**, e1004961 (2015).
654 37. Ishikawa-Ankerhold, H. C., Ankerhold, R. & Drummen, G. P. C. Advanced
655 fluorescence microscopy techniques--FRAP, FLIP, FLAP, FRET and FLIM. *Mol.*
656 *Basel Switz.* **17**, 4047–4132 (2012).
657 38. Becker, J. T. & Sherer, N. M. Subcellular Localization of HIV-1 gag-pol mRNAs

658 Regulates Sites of Virion Assembly. *J. Virol.* **91**, (2017).
659 39. Chen, J. *et al.* High efficiency of HIV-1 genomic RNA packaging and heterozygote
660 formation revealed by single virion analysis. *Proc. Natl. Acad. Sci. U. S. A.* **106**,
661 13535–13540 (2009).
662 40. Desimmie, B. A. *et al.* APOBEC3 proteins can copackage and comutate HIV-1
663 genomes. *Nucleic Acids Res.* **44**, 7848–7865 (2016).
664 41. Accola, M. A., Strack, B. & Göttlinger, H. G. Efficient particle production by minimal
665 Gag constructs which retain the carboxy-terminal domain of human
666 immunodeficiency virus type 1 capsid-p2 and a late assembly domain. *J. Virol.* **74**,
667 5395–5402 (2000).
668 42. Reed, J. C. *et al.* HIV-1 Gag co-opts a cellular complex containing DDX6, a helicase
669 that facilitates capsid assembly. *J. Cell Biol.* **198**, 439–456 (2012).
670 43. Barajas, B. C. *et al.* Identifying the assembly intermediate in which Gag first
671 associates with unspliced HIV-1 RNA suggests a novel model for HIV-1 RNA
672 packaging. *PLoS Pathog.* **14**, e1006977 (2018).
673 44. Soto-Rifo, R. *et al.* HIV-2 genomic RNA accumulates in stress granules in the
674 absence of active translation. *Nucleic Acids Res.* **42**, 12861–12875 (2014).
675 45. Bann, D. V., Beyer, A. R. & Parent, L. J. A murine retrovirus co-Opts YB-1, a
676 translational regulator and stress granule-associated protein, to facilitate virus
677 assembly. *J. Virol.* **88**, 4434–4450 (2014).
678 46. Goodier, J. L., Zhang, L., Vetter, M. R. & Kazazian, H. H. LINE-1 ORF1 protein
679 localizes in stress granules with other RNA-binding proteins, including components
680 of RNA interference RNA-induced silencing complex. *Mol. Cell. Biol.* **27**, 6469–6483
681 (2007).
682 47. Larsen, L. S. Z. *et al.* Ty3 nucleocapsid controls localization of particle assembly. *J.*
683 *Virol.* **82**, 2501–2514 (2008).
684 48. Kennedy, E. M. *et al.* Posttranscriptional m(6)A Editing of HIV-1 mRNAs Enhances
685 Viral Gene Expression. *Cell Host Microbe* **19**, 675–685 (2016).
686 49. Lichinchi, G. *et al.* Dynamics of the human and viral m(6)A RNA methylomes during
687 HIV-1 infection of T cells. *Nat. Microbiol.* **1**, 16011 (2016).
688 50. Tirumuru, N. *et al.* N(6)-methyladenosine of HIV-1 RNA regulates viral infection and
689 HIV-1 Gag protein expression. *eLife* **5**, (2016).
690 51. Courtney, D. G. *et al.* Epitranscriptomic Addition of m5C to HIV-1 Transcripts
691 Regulates Viral Gene Expression. *Cell Host Microbe* **26**, 217-227.e6 (2019).
692 52. Chesebro, B., Wehrly, K., Nishio, J. & Perryman, S. Macrophage-tropic human
693 immunodeficiency virus isolates from different patients exhibit unusual V3 envelope
694 sequence homogeneity in comparison with T-cell-tropic isolates: definition of critical
695 amino acids involved in cell tropism. *J. Virol.* **66**, 6547–6554 (1992).
696 53. Adachi, A. *et al.* Production of acquired immunodeficiency syndrome-associated
697 retrovirus in human and nonhuman cells transfected with an infectious molecular
698 clone. *J. Virol.* **59**, 284–291 (1986).
699 54. Connor, R. I., Chen, B. K., Choe, S. & Landau, N. R. Vpr is required for efficient
700 replication of human immunodeficiency virus type-1 in mononuclear phagocytes.
701 *Virology* **206**, 935–944 (1995).
702 55. Simon, J. H. *et al.* The regulation of primate immunodeficiency virus infectivity by Vif
703 is cell species restricted: a role for Vif in determining virus host range and cross-

704 species transmission. *EMBO J.* **17**, 1259–1267 (1998).
705 56. Femino, A. M., Fay, F. S., Fogarty, K. & Singer, R. H. Visualization of single RNA
706 transcripts in situ. *Science* **280**, 585–590 (1998).
707 57. Shcherbakova, D. M. & Verkhusha, V. V. Near-infrared fluorescent proteins for
708 multicolor in vivo imaging. *Nat. Methods* **10**, 751–754 (2013).
709 58. Sladitschek, H. L. & Neveu, P. A. MXS-Chaining: A Highly Efficient Cloning Platform
710 for Imaging and Flow Cytometry Approaches in Mammalian Systems. *PloS One* **10**,
711 e0124958 (2015).
712 59. Subach, O. M., Cranfill, P. J., Davidson, M. W. & Verkhusha, V. V. An enhanced
713 monomeric blue fluorescent protein with the high chemical stability of the
714 chromophore. *PloS One* **6**, e28674 (2011).
715 60. Sherer, N. M. *et al.* Evolution of a species-specific determinant within human CRM1
716 that regulates the post-transcriptional phases of HIV-1 replication. *PLoS Pathog.* **7**,
717 e1002395 (2011).
718 61. Hardin, J. Imaging embryonic morphogenesis in C. elegans. *Methods Cell Biol.* **106**,
719 377–412 (2011).
720 62. Schindelin, J. *et al.* Fiji: an open-source platform for biological-image analysis. *Nat.*
721 *Methods* **9**, 676–682 (2012).
722 63. Garcia-Miranda, P. *et al.* Stability of HIV Frameshift Site RNA Correlates with
723 Frameshift Efficiency and Decreased Virus Infectivity. *J. Virol.* **90**, 6906–6917
724 (2016).

725 **FIGURE LEGENDS**

726 **Fig. 1. Tracking the HIV-1 replication cycle using a YFP-A3G biosensor cell line. a**
727 HeLa.YFP-A3G cells showing diffuse and punctate (processing bodies, PB, white arrows)
728 distribution of YFP-A3G at steady-state (left) and accumulation into stress granules (SGs,
729 magenta arrows) following arsenite treatment (right, Ars). **b** Schematic of Vif-competent
730 (Vif+) or deficient (Vifxx) HIV-1 NL4-3 Env-, Vpr-, expressing CFP as a reporter of
731 infection. **c** Single-round infection confirms YFP-A3G dependent restriction of HIV-1 in
732 the absence of Vif. 293T.YFP-A3G cells were transfected with the indicated HIV-1
733 reporter viruses with or without co-expression of a plasmid encoding Vif-mCherry. Cells
734 and virus particles (*n*=3) were harvested at 48 h post-transfection and analyzed by
735 quantitative immunoblot using anti-$p24_{Gag}$, anti-YFP, and anti-HSP90 (loading control)
736 antisera. **d** Representative images from long-term time-lapse imaging showing
737 degradation of YFP-A3G upon HIV-1 Vif+ CFP infection and eventual Vif-dependent
738 G2/M arrest. **e** Quantification of movies (IntDen) represented in d (Vif+, solid lines) and **f**
739 (Vifxx, dashed lines). Cells from 3 independent experiments (*n*=33) with ≥16 hours per
740 cell (1 image/hour). **f** Representative images from long-term time-lapse imaging of YFP-
741 A3G upon HIV-1 Vifxx CFP infection. Magenta boxes highlight zoomed regions of interest
742 (ROIs) shown below and white arrows highlight YFP-A3G clustering at PM. **g** Fixed cell
743 images show Gag and *gagpol* mRNA (viral RNA genomes) accumulating with YFP-A3G
744 at cell periphery. White arrows highlight cell-peripheral clusters of YFP-A3G, Gag, and
745 genome. **h** TSEM images showing virus particles clustering in the extracellular space
746 after budding from HeLa.YFP-A3G cells infected with either Vif+ or Vifxx viruses. All scale

747 bars in fluorescent images = 10μm and in TSEM = 100nm. Error bars represent standard
748 deviation of the mean.
749
750 **Fig. 2. HIV-1 infection has little to no impact on P-bodies or stress granules**. **a**
751 HeLa.YFP-TIA1 cells showing steady-state distribution (vehicle, left) and accumulation
752 into SGs (magenta arrows) following arsenite treatment (right, Ars). **b** Representative
753 images of time-lapse imaging showing induction of SGs during infection by RVA16
754 (MOI=10). **c** Time-lapse images showing no effect on YFP-TIA1 distribution following
755 Vifxx CFP infection, quantified in **d** for >400 HeLa.YFP-A3G (black bars) and HeLa.YFP-
756 TIA1 (gray bars) cells per condition, combined from three independent experiments. **e**
757 Time-lapse images showing no effect on CFP-DCP1a following Vifxx mCh infection,
758 quantified in **f** for 30 cells from 3 movies at ~18 hpi (YFP-A3G, black bars; CFP-DCP1a,
759 white bars). **g** HeLa.YFP-A3G infected with Vifxx CFP and treated with Ars to induce SGs
760 at 24 hpi and quantified in **h** for at least 100 infected cells from three independent
761 experiments. Magenta arrows highlight SGs present in infected cells. **i** Simultaneous
762 FISH/IF to detect *gagpol* mRNA and Gag show HIV RNA genomes accumulating in SGs
763 in HIV infected cells following Ars treatment. Magenta arrows highlight SGs present in
764 infected cells. All scale bars in fluorescent images = 10μm. Error bars represent standard
765 deviation of the mean.
766
767 **Fig. 3. HIV-1 RNA genomes but not Gag regulate A3G subcellular localization. a and**
768 **c** Schematic Vif+ and Vifxx two-color self-tagging virus encoding Gag-CFP, 24xMSL, and
769 MS2-RFP. **b** and **d** Time-lapse images of cells expressing Vif+ and Vifxx two-color HIV

770 constructs showing nuclear export of MS2-RFP tagged genomes, YFP-A3G degradation
771 (**b,** Vif+) or localization with MS2-RFP (**d,** Vifxx), and Gag-CFP expression and
772 accumulation into virus particles at the PM (white arrows). **e** and **f** Quantification of YFP-
773 A3G degradation and MS2-RFP cytoplasmic accumulation (**e**) and Gag-CFP expression
774 (**f**) during expressing of Vif+ two-color HIV construct. Cells (*n*=31) from three independent
775 experiments wherein individual cells that could be tracked for at least 17 h (1 image/hour).
776 Black lines highlight the ~3 h window of YFP-A3G degradation. T=0 represents onset of
777 MS2-RFP expression. **g** Schematic of "genome only" and "Gag only" constructs. **h**
778 Representative images from before (top) and after (before) photobleaching in HeLa.YFP-
779 A3G cells expressing "genome only" construct. White dashed circles represent regions of
780 targeted photobleaching. **i** Quantification of YFP-A3G fluorescence recovery experiments
781 and zoomed inset of time period over first 80 seconds after photobleaching. All scale bars
782 in fluorescent images = 10μm. Error bars represent standard deviation of the mean.
783

784 **Fig. 4. Viral RNA Genome-A3G interactions are sufficiently strong to redistribute**
785 **A3G to unnatural subcellular locales. a** Schematic of In Cell RNA-protein Interaction
786 Protocol (IC-IP). **b** Schematic of MS2-iRFP constructs used for "targeting" (top) and
787 representative images of MS2-iRFP and YFP-A3G localization in the absence of mRNAs
788 encoding MSL cassette. White arrows point to characteristic subcellular targets of Src-
789 (vesicles) and Lifeact- (filamentous actin) MS2-iRFP. **c** Schematic of IC-IP RNA Bait –
790 Vifxx two-color self-tagging HIV construct. **d** Representative images showing Free MS2-
791 iRFP-NLS, MS2-RFP-NLS, YFP-A3G, and Gag-CFP accumulating at PM-adjacent
792 assembly sites (top). (Middle) Src-MS2-iRFP accumulates at intracellular/perinuclear

793 vesicles, recruits MS2-RFP-tagged RNA genomes, YFP-A3G, and Gag-CFP. (Bottom)
794 Lifeact-MS2-iRFP induces similar accumulation at actin filaments. Region of interest
795 (ROI) shows YFP-A3G signal in dashed white boxes with arrows highlighting assembly
796 sites (top), vesicles (middle), and linear filaments (bottom). **e** Quantification of re-
797 localization of YFP-A3G phenotypes (*n* = > 90 cells per condition) in the presence of NLS,
798 Src-, and Lifeact-MS2 targeting constructs and **f** percentages of YFP-A3G per cell signal
799 (IntDen) relocalized by Src- and Lifeact-MS2 constructs (*n* > 6). All scale bars in
800 fluorescent images = 10μm, except in A3G ROI insets scale bars = 1μm. Error bars
801 represent standard deviation of the mean.
802
803 **Fig. 5. Recruitment of YFP-A3G is specific to HIV-1 RNA genome, Gag-independent,**
804 **and occurs long before the onset of virus particle assembly. a and c** Schematics of
805 "genome only" and "Gag only" IC-IP bait constructs, respectively. **b** Representative
806 images showing normal co-distribution of MS2-RFP tagged RNA genomes and YFP-A3G
807 (top) and retargeting of YFP-A3G to intracellular vesicles with RNA genomes by Src-MS2-
808 iRFP (bottom). **d** Representative images showing Src-MS2-RFP accumulating at
809 intracellular vesicles and a complete lack of YFP-A3G at these same sites (white arrow).
810 **e** Time-lapse images of cells expressing "genome only" construct retargeted by Src-MS2-
811 iRFP over a period of 4 hours. T=0 represents the first detection of MS2-RFP genome
812 proxy. Arrow shows accumulation of YFP-A3G at Src-MS2-iRFP+ vesicles as early as 2
813 hours after the onset of MS2-RFP expression. All scale bars in fluorescent images =
814 10μm.
815

816 **Fig. 6. Membrane-targeted APOBEC3G recruits HIV-1 RNA genomes and can inhibit**
817 **virus particle production. a** Schematic of Reciprocal IC-IP using Src-YFP-A3G targeted
818 to intracellular membranes. **b** and **c** Schematic of Vifxx two-color HIV (**b**) and "genome
819 only" (**c**) constructs and representative images showing Src-YFP-A3G (**b**) or Src-CFP-
820 A3G (**c**) recruiting MS2-RFP tagged genomes to intracellular vesicles (white arrows). **d**
821 Schematic of Vifxx Luc HIV infectious single-cycle virus used to infect HeLa.Src-YFP-
822 A3G cells and representative images of FISH/IF detecting *gag-pol* mRNA and Gag p-24,
823 respectively. White arrows highlight sites where Src-YFP-A3G has recruited *bona fide*
824 HIV RNA genomes. **e** Western blot showing dose-dependent inhibition of HIV virus
825 particle assembly and production from HEK293T cells transfected with Vifxx two-color
826 construct, Src-MS2-YFP (lanes 1 and 2), YFP-A3G (lane 3) and Src-YFP-A3G (lanes 4
827 and 5). Graph shows relative release factor as the ratio of Gag in virus-like particles
828 (VLPs) divided by Gag in cellular lysates quantified from three independent experiments.
829 All scale bars in fluorescent images = 10μm. Error bars represent standard deviation of
830 the mean.
831
832 **Fig. 7. Cytoplasmic A3G-genome interactions promote consistent per virion**
833 **delivery of A3G into progeny virions. a** Schematics of constructs used in single virion
834 analysis (SVA) studies. **b** Western blot showing cellular expression, YFP-A3G packaging,
835 and Gag assembly and release of constructs depicted in a. **c** Representative images of
836 single fluorescent virion images harvested from HEK293T.YFP-A3G cell line. Scale bar
837 = 500nm. **d** Quantification of SVA for each of the four constructs showing percent of
838 virions with MS2-RFP signal (pink) and YFP-A3G (green). Error bars represent standard

839 deviation of the mean (*n* > 13,000 virions per condition). **e** Relative YFP-A3G signal per
840 virion or virus-like particle derived from Vifxx two-color or COGag conditions. Relative
841 values are normalized to the mean value for Vifxx with means (solid lines) and 25th and
842 75th quartiles (dashed lines) indicated.

843 **SUPPLEMENTARY MATERIAL**

844

845 **Fig. S1. Graphical abstract.** Summary of single-cell live imaging approaches used and
846 key findings.

847

848 **Video 1. Time-lapse imaging of HeLa-.FP-A3G cells infected with Vif+ HIV-1/CFP**
849 **virus.** Multi-channel images of HeLa.YFP-A3G cells were acquired every 60 minutes for
850 49h after infection. In the highlighted cell, viral gene expression (cyan) is detected ~16hpi
851 with YFP-A3G degradation green0 at 21hpi. This cell rounds up at 28 hpi consistent with
852 Vif-induced G2/M cell cycle arrest.

853

854 **Video 2. Time-lapse imaging of HeLa.YFP-A3G cells infected with Vifxx HIV-1/CFP**
855 **virus.** Multi-channel images were acquired every 60 minutes for 49h after infection. In the
856 highlighted cell, viral gene expression (cyan) is detected ~19hpi with detection of YFP-
857 A3G (green) at virus particles (arrows) starting at ~25hpi. An example of a transfer event
858 wherein a large cluster of YFP-A3G+ virus particles is released from an infected cell is
859 highlighted (arrows) at 32-36hpi.

860

861 **Video 3. Time-lapse imaging of HeLa.YFP-TIA1 cells infected with Rhinovirus A16.**
862 Multi-channel images were acquired every 30 minutes after addition of RVA16 (MOI~10).
863 The first instances of SG formation (YFP-TIA1 in green) are evident at ~11hpi.

864

865 **Video 4. Time-lapse imaging of HeLa.YFP-A3G cells expressing the two-color Vif+**
866 **Gag-CFP/MS2-RFP HIV-1 reporter virus.** Multi-channel images were acquired every 60
867 minutes for 24h beginning ~4h post-transfection. Left panel shows genome tracked using
868 MS2-RFP (magenta), with nuclear export detected at T=4h just prior to the onset of Gag-
869 CFP (cyan) expression (right panel) and YFP-A3G (green) degradation (center panel).
870
871 **Video 5. Time-lapse imaging of HeLa.YFP-A3G cells expressing the two-color Vifxx**
872 **Gag-CFP/MS2-RFP HIV-1 reporter virus.** Multi-channel images were acquired every 60
873 minutes for 24 hours beginning ~4 hours post-transfection. Left panel shows genome
874 tracked using MS2-RFP (magenta), with nuclear export detected at T=6h just prior to the
875 onset of Gag-CFP (cyan) expression (right panel) and co-accumulation of YFP-A3G
876 (green, center panel) with genome (MS2-RFP) and Gag-CFP at the plasma membrane
877 (at putative sites of virus particle assembly).
878
879 **Video 6. Time-lapse imaging of HeLa.YFP-A3G cells co-expressing "genome only"**
880 **MS2-RFP HIV-1 reporter virus with the Src-MS2-iRFP targeter (orange).** Multi-
881 channel images were acquired every 60 minutes for 15h starting ~4h post-transfection.
882 MS2-RFP tracked genomes (magenta, central panel) are first observed at T=0, with both
883 genomes and YFP-A3G (green, right panel) immediately recruited to perinuclear vesicles,
884 co-localizing with the Src-MS2-iRFP targeter (yellow, left panel). Video demonstrates that
885 genomes have marked effects on YFP-A3G trafficking in the cytosol even at the earliest
886 time points post-genome nuclear export.

# FIGURE 1

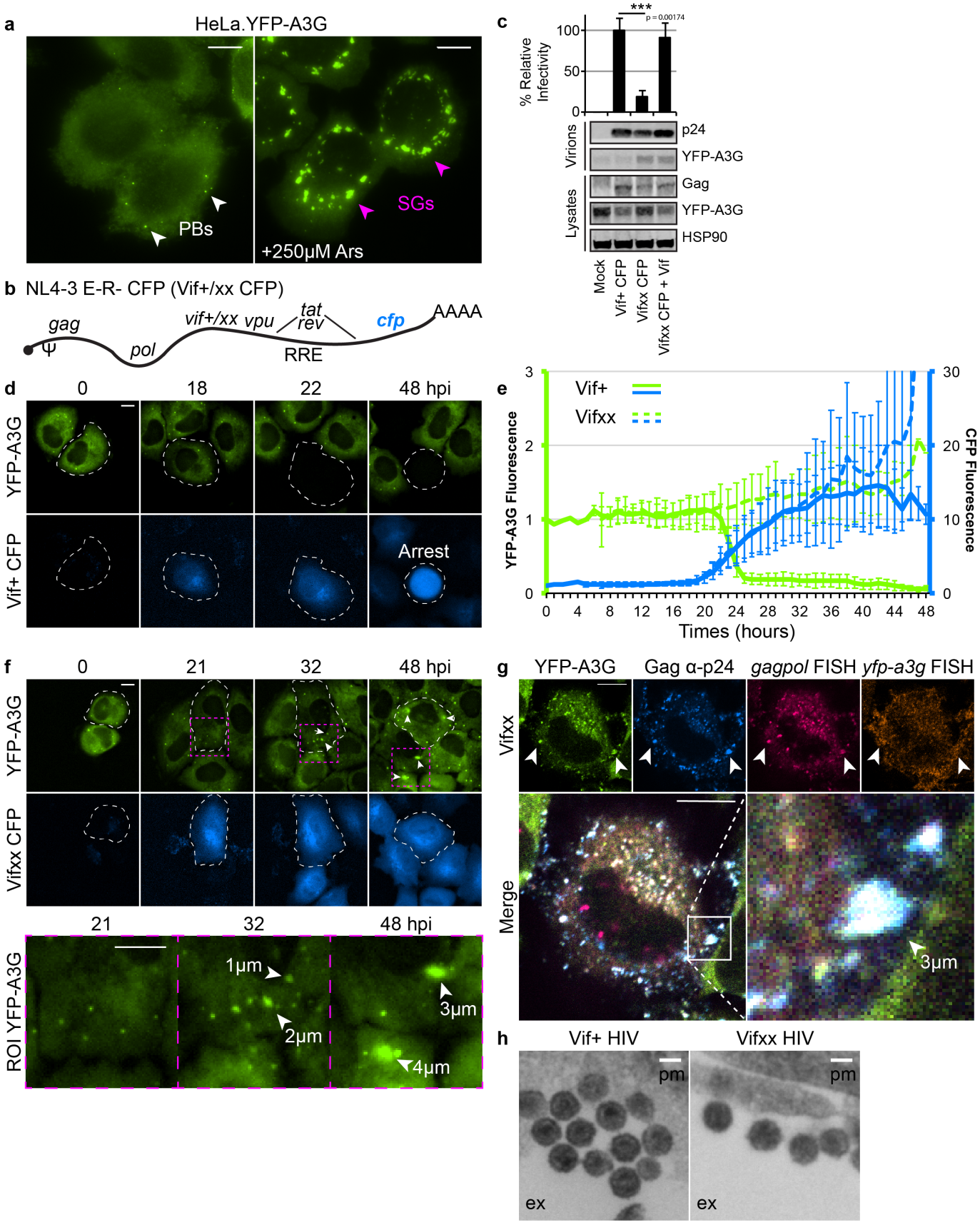
a
HeLa.YFP-A3G
PBs
SGs
+250μM Ars
b
NL4-3 E-R- CFP (Vif+/xx CFP)
gag
Ψ
pol
vif+/xx vpu
tat
rev
RRE
cfp
AAAA
c
% Relative Infectivity
***
p = 0.00174
100
50
0
Virions
Lysates
p24
YFP-A3G
Gag
YFP-A3G
HSP90
Mock
Vif+ CFP
Vifxx CFP
Vifxx CFP + Vif
d
0
18
22
48 hpi
YFP-A3G
Vif+ CFP
Arrest
e
Vif+
Vifxx
YFP-A3G Fluorescence
CFP Fluorescence
Times (hours)
f
0
21
32
48 hpi
YFP-A3G
Vifxx CFP
ROI YFP-A3G
1μm
2μm
3μm
4μm
g
YFP-A3G
Gag α-p24
gagpol FISH
yfp-a3g FISH
Vifxx
Merge
3μm
h
Vif+ HIV
Vifxx HIV
pm
ex

# FIGURE 2

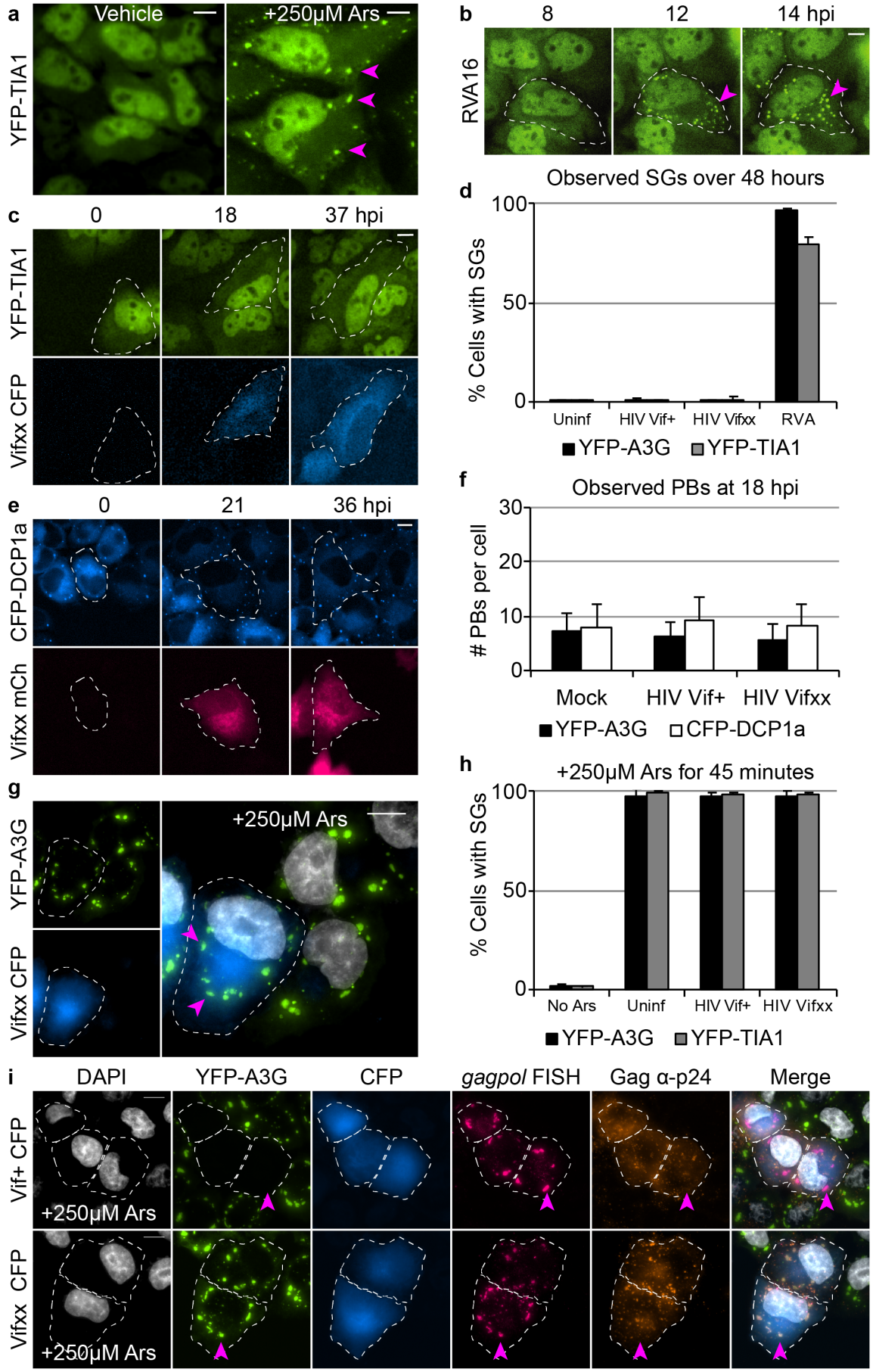
a
Vehicle
+250μM Ars
YFP-TIA1
b
8
12
14 hpi
RVA16
c
0
18
37 hpi
YFP-TIA1
Vifxx CFP
d
Observed SGs over 48 hours
% Cells with SGs
100
50
0
Uninf
HIV Vif+
HIV Vifxx
RVA
YFP-A3G
YFP-TIA1
e
0
21
36 hpi
CFP-DCP1a
Vifxx mCh
f
Observed PBs at 18 hpi
# PBs per cell
30
20
10
0
Mock
HIV Vif+
HIV Vifxx
YFP-A3G
CFP-DCP1a
g
+250μM Ars
YFP-A3G
Vifxx CFP
h
+250μM Ars for 45 minutes
% Cells with SGs
100
50
0
No Ars
Uninf
HIV Vif+
HIV Vifxx
YFP-A3G
YFP-TIA1
i
DAPI
YFP-A3G
CFP
gagpol FISH
Gag α-p24
Merge
Vif+ CFP
+250μM Ars
Vifxx CFP
+250μM Ars

# FIGURE 3

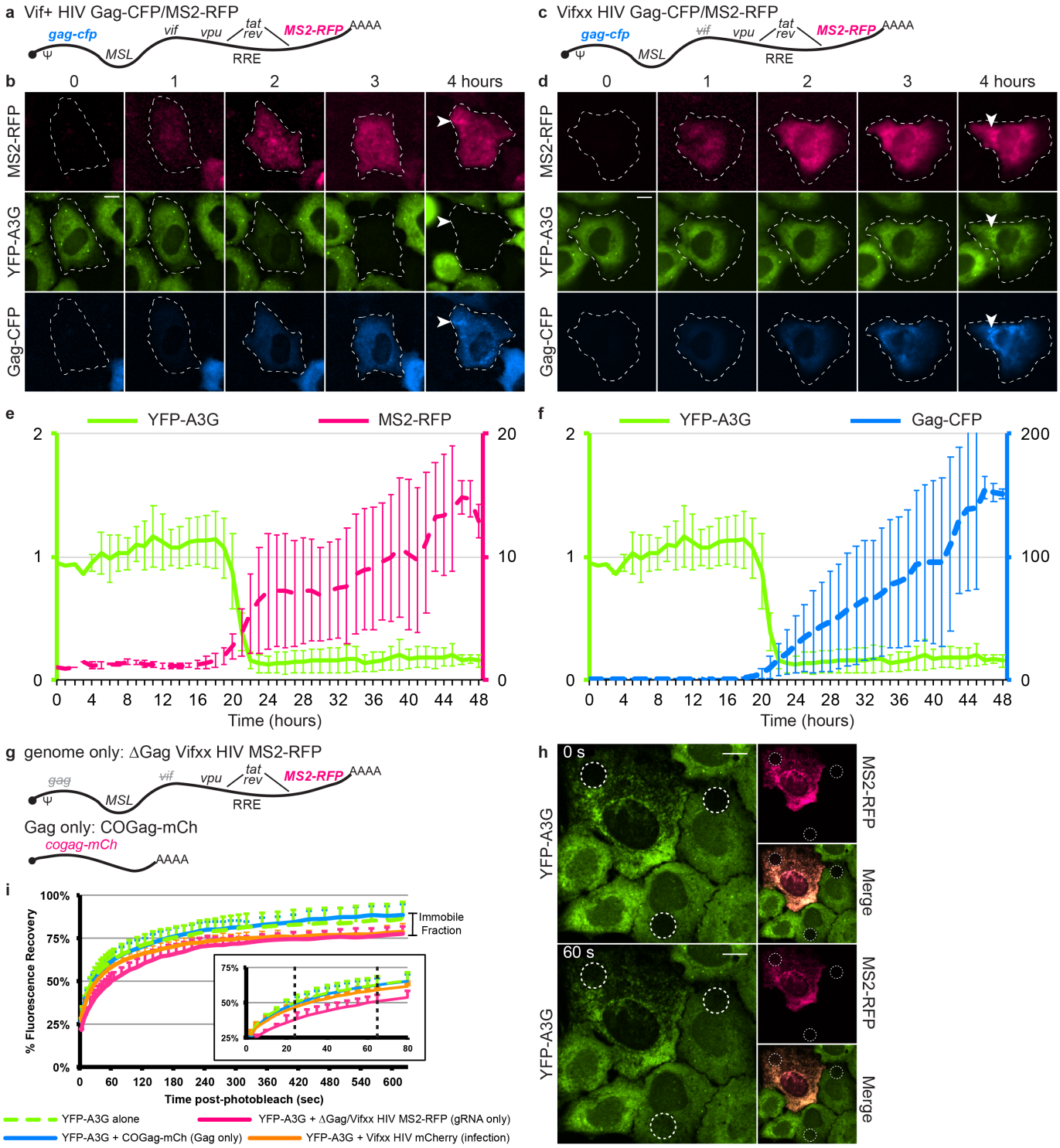
a Vif+ HIV Gag-CFP/MS2-RFP
gag-cfp
Ψ
MSL
vif
vpu
tat
rev
RRE
MS2-RFP
AAAA
c Vifxx HIV Gag-CFP/MS2-RFP
b
0
1
2
3
4 hours
MS2-RFP
YFP-A3G
Gag-CFP
d
e
YFP-A3G
MS2-RFP
Time (hours)
f
Gag-CFP
g genome only: ΔGag Vifxx HIV MS2-RFP
gag
Gag only: COGag-mCh
cogag-mCh
i
% Fluorescence Recovery
Immobile Fraction
Time post-photobleach (sec)
YFP-A3G alone
YFP-A3G + ΔGag/Vifxx HIV MS2-RFP (gRNA only)
YFP-A3G + COGag-mCh (Gag only)
YFP-A3G + Vifxx HIV mCherry (infection)
h
0 s
60 s
Merge

# FIGURE 4

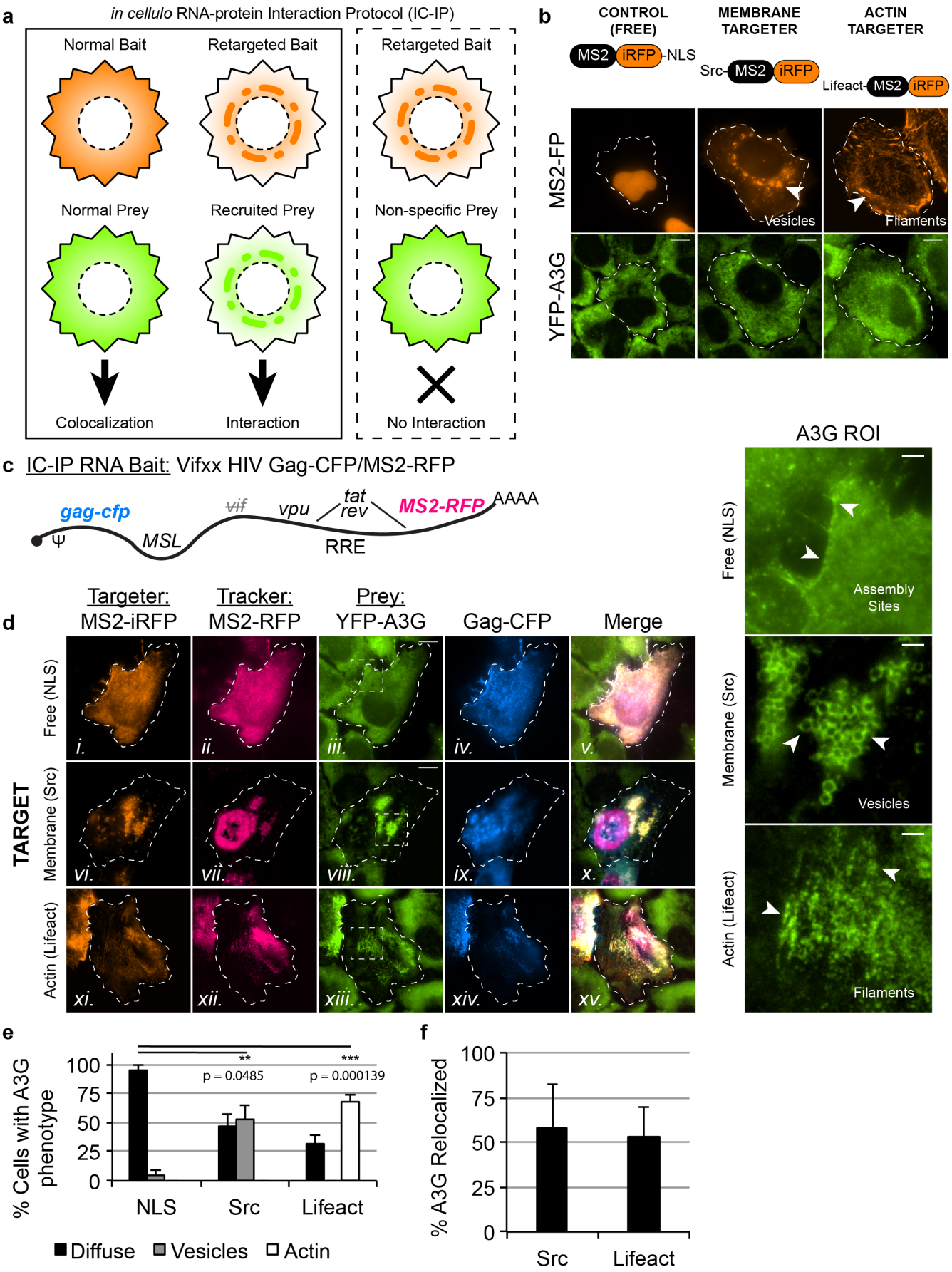
a
in cellulo RNA-protein Interaction Protocol (IC-IP)
Normal Bait
Retargeted Bait
Retargeted Bait
Normal Prey
Recruited Prey
Non-specific Prey
Colocalization
Interaction
No Interaction
b
CONTROL (FREE)
MEMBRANE TARGETER
ACTIN TARGETER
MS2 iRFP -NLS
Src- MS2 iRFP
Lifeact- MS2 iRFP
MS2-FP
YFP-A3G
Vesicles
Filaments
c IC-IP RNA Bait: Vifxx HIV Gag-CFP/MS2-RFP
gag-cfp
vif
vpu
tat
rev
MS2-RFP
AAAA
Ψ
MSL
RRE
d
Targeter: MS2-iRFP
Tracker: MS2-RFP
Prey: YFP-A3G
Gag-CFP
Merge
TARGET
Free (NLS)
Membrane (Src)
Actin (Lifeact)
i.
ii.
iii.
iv.
v.
vi.
vii.
viii.
ix.
x.
xi.
xii.
xiii.
xiv.
xv.
A3G ROI
Free (NLS)
Assembly Sites
Membrane (Src)
Vesicles
Actin (Lifeact)
Filaments
e
% Cells with A3G phenotype
100
75
50
25
0
**
p = 0.0485
***
p = 0.000139
NLS
Src
Lifeact
Diffuse
Vesicles
Actin
f
% A3G Relocalized
100
75
50
25
0
Src
Lifeact

# FIGURE 5

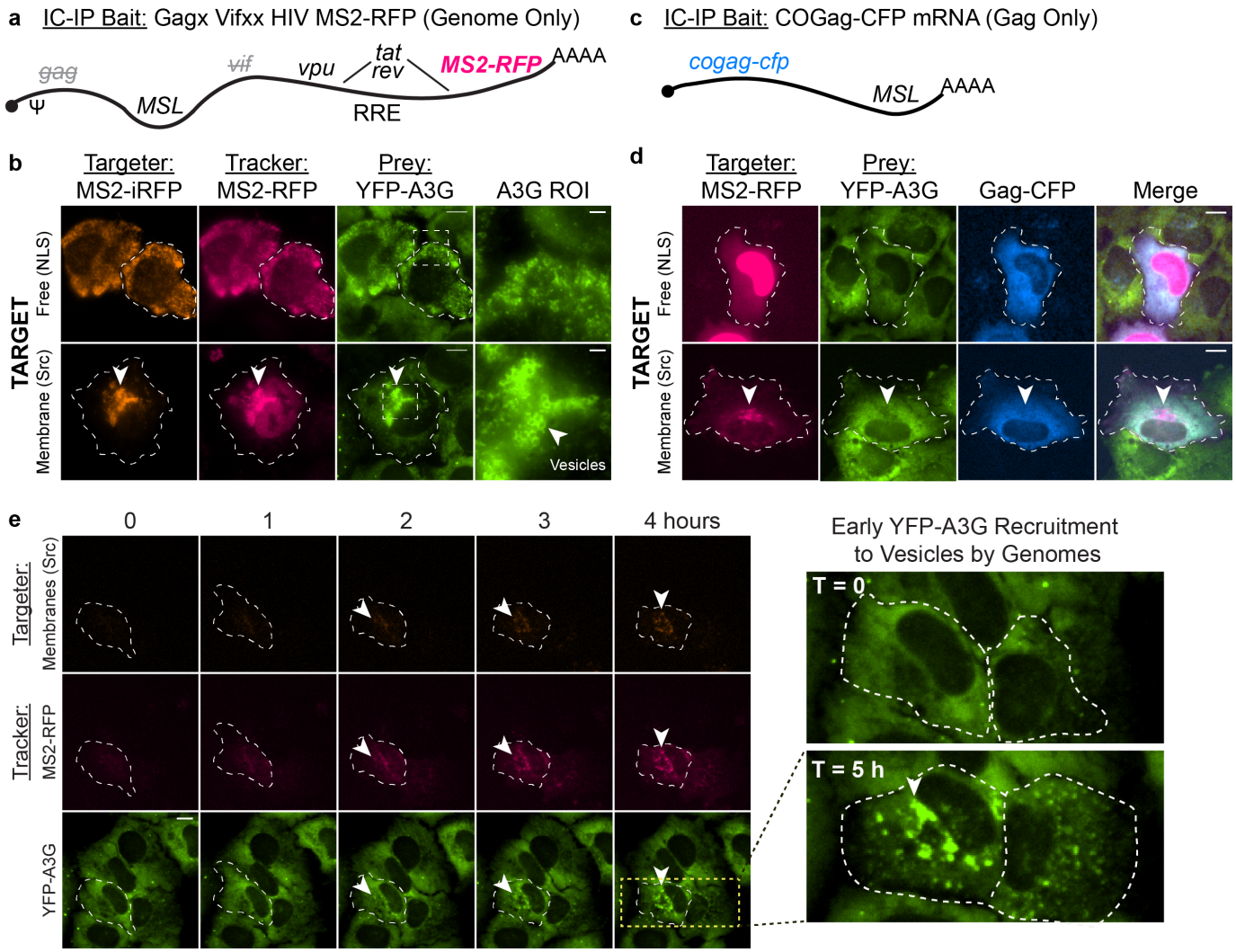
a
IC-IP Bait: Gagx Vifxx HIV MS2-RFP (Genome Only)
gag
vif
vpu
tat
rev
MS2-RFP
AAAA
Ψ
MSL
RRE
c
IC-IP Bait: COGag-CFP mRNA (Gag Only)
cogag-cfp
MSL
AAAA
b
Targeter: MS2-iRFP
Tracker: MS2-RFP
Prey: YFP-A3G
A3G ROI
TARGET
Free (NLS)
Membrane (Src)
Vesicles
d
Targeter: MS2-RFP
Prey: YFP-A3G
Gag-CFP
Merge
TARGET
Free (NLS)
Membrane (Src)
e
0
1
2
3
4 hours
Targeter: Membranes (Src)
Tracker: MS2-RFP
YFP-A3G
Early YFP-A3G Recruitment to Vesicles by Genomes
T = 0
T = 5 h

# FIGURE 6

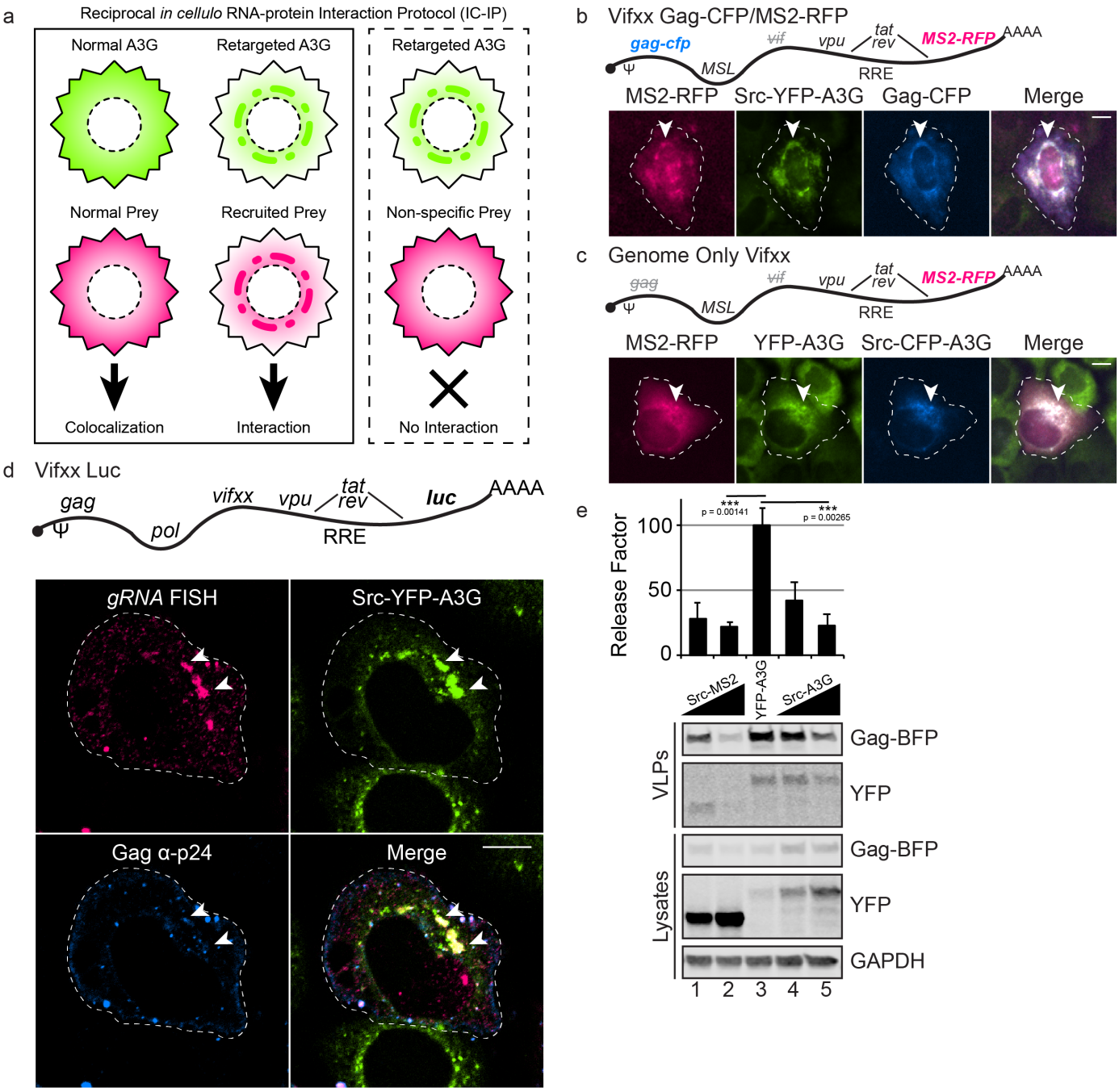
a
Reciprocal in cellulo RNA-protein Interaction Protocol (IC-IP)
Normal A3G
Retargeted A3G
Retargeted A3G
Normal Prey
Recruited Prey
Non-specific Prey
Colocalization
Interaction
No Interaction
b
Vifxx Gag-CFP/MS2-RFP
gag-cfp
vif
vpu
tat
rev
MS2-RFP
AAAA
Ψ
MSL
RRE
MS2-RFP
Src-YFP-A3G
Gag-CFP
Merge
c
Genome Only Vifxx
gag
vif
vpu
tat
rev
MS2-RFP
AAAA
Ψ
MSL
RRE
MS2-RFP
YFP-A3G
Src-CFP-A3G
Merge
d
Vifxx Luc
gag
vifxx
vpu
tat
rev
luc
AAAA
Ψ
pol
RRE
gRNA FISH
Src-YFP-A3G
Gag α-p24
Merge
e
Release Factor
100
50
0
***
p = 0.00141
***
p = 0.00265
Src-MS2
YFP-A3G
Src-A3G
VLPs
Gag-BFP
YFP
Lysates
Gag-BFP
YFP
GAPDH
1
2
3
4
5

# FIGURE 7

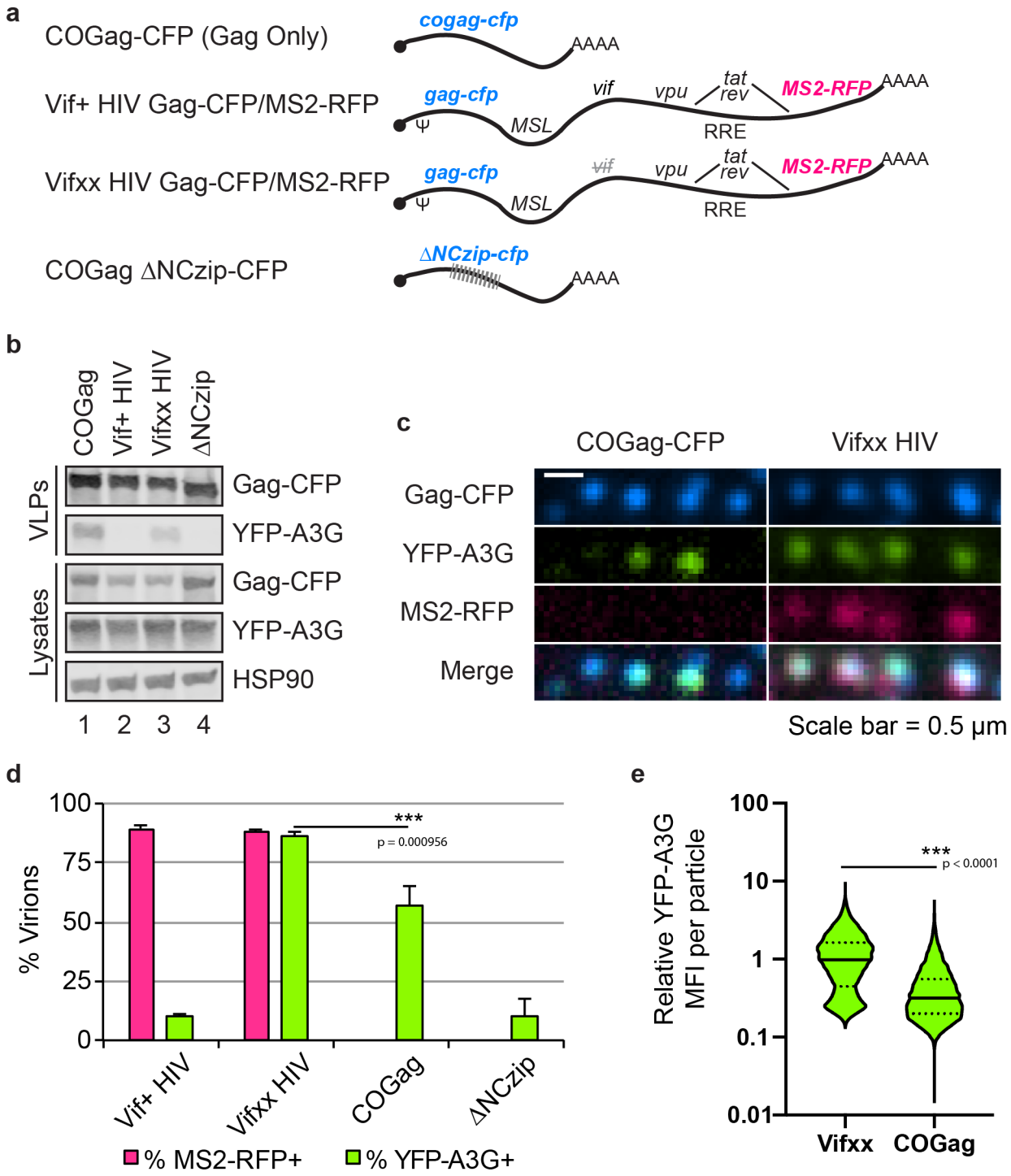
a
COGag-CFP (Gag Only)
cogag-cfp
AAAA
Vif+ HIV Gag-CFP/MS2-RFP
gag-cfp
Ψ
MSL
vif
vpu
tat
rev
RRE
MS2-RFP
AAAA
Vifxx HIV Gag-CFP/MS2-RFP
gag-cfp
Ψ
MSL
vif
vpu
tat
rev
RRE
MS2-RFP
AAAA
COGag ΔNCzip-CFP
ΔNCzip-cfp
AAAA
b
COGag
Vif+ HIV
Vifxx HIV
ΔNCzip
VLPs
Lysates
Gag-CFP
YFP-A3G
Gag-CFP
YFP-A3G
HSP90
1 2 3 4
c
COGag-CFP
Vifxx HIV
Gag-CFP
YFP-A3G
MS2-RFP
Merge
Scale bar = 0.5 µm
d
% Virions
100
75
50
25
0
***
p = 0.000956
Vif+ HIV
Vifxx HIV
COGag
ΔNCzip
% MS2-RFP+
% YFP-A3G+
e
Relative YFP-A3G MFI per particle
100
10
1
0.1
0.01
***
p < 0.0001
Vifxx
COGag